A Photometric and Radial-Velocity Study of the Open Cluster NGC 7789

by

Munhwan Gim
B.Sc., Yonsei University, 1988
M.Sc., Yonsei University, 1990

A Thesis Submitted in Partial Fulfillment of the
Requirements for the Degree of

MASTER OF SCIENCE

in the Department of Physics and Astronomy

We accept this thesis as conforming
to the required standard.

[redacted]

Dr. D.A. VandenBerg, Co-supervisor (Department of Physics and Astronomy)

[redacted]

Dr. J.E. Hesser, Co-supervisor (Dominion Astrophysical Observatory (DAO))

[redacted]

Dr. P.B. Stetson, Co-supervisor (DAO)

[redacted]

Dr. J.B. Tatum, Departmental Member (Department of Physics and Astronomy)

[redacted]

Dr. C.G. Morgan, Outside Member (Department of Philosophy)

[redacted]

Dr. F. Grundahl, External Examiner (DAO)

Co-supervisors: Dr. D.A. VandenBerg, Dr. J.E. Hesser, and Dr. P.B. Stetson

Abstract

A $(V, V-I)$–diagram, reaching $V \sim 21$ ($M_V \sim 9$), has been derived for the intermediate-age open cluster NGC 7789 from CCD observations of more than 15,000 stars within ≈ 18 arcmin of the cluster center. A prominent clump of core helium-burning stars is evident at $V = 13.0$ and the upper end of the main sequence shows a fairly pronounced curvature to the red, which indicates significant convective core overshooting. Interestingly, if sufficient overshooting is assumed in order to match the main-sequence data, it is not possible to reproduce the cluster's extended giant branch unless the cluster age is at least 1.6 Gyr (assuming a metallicity in the range $-0.2 \leq$ [Fe/H] ≤ 0.0). This, in turn, requires that the cluster have an apparent distance modulus $(m-M)_V \leq 12.2$. We infer a reddening $0.35 \leq E(V-I) \leq 0.38$.

A total of 597 radial-velocity observations for 112 giant stars, which have been obtained since 1979 with the radial velocity spectrometer at the Dominion Astrophysical Observatory, shows that the mean radial velocity is -54.9 ± 0.12 km s^{-1} and the dispersion is 0.86 km s^{-1}, estimated from 50 constant-velocity stars selected as members. Twenty-five stars (32%) among 78 members are possible radial-velocity variable stars, but no orbits are determined because of the sparse sampling. Seventeen stars are radial-velocity non-members, while membership estimates for six stars are uncertain. There is a hint that the observed velocity dispersion falls off at large radius. The known radial-velocity variables also seem to be more centrally-concentrated

than members with constant velocity, suggesting that mass segregation is being detected.

Examiners:

[redacted]

Dr. D.A. VandenBerg, Co-supersvisor (Dept. of Physics and Astronomy)

[redacted]

Dr. J.E. Hesser, Co-supervisor (DAO)

[redacted]

Dr. P.B. Stetson, Co-supervisor (DAO)

[redacted]

Dr. J.B. Tatum, Departmental Member (Dept. of Physics and Astronomy)

[redacted]

Dr. C.G. Morgan, Outside Member (Dept. of Philosophy)

[redacted]

Dr. F. Grundahl, External Member (DAO)

Contents

List of Tables

List of Figures

Acknowledgments

I would like to thank Don A. VandenBerg, Peter B. Stetson, and James E. Hesser for their guidance, encouragement, financial support throughout this work, and for many other things.

I also thank Robert D. McClure for his guidance on using the radial-velocity scanner at the DAO and for his careful reading and advice regarding part of this thesis. Without the radial-velocity data which had been observed by Jim and Bob since 1979, this work would have not been possible. I also would like to thank all DAO night assistants - Les Saddlemyer, Doug Bond and Frank Younger - for their help whenever it was needed. I am grateful to Dave Zurek for his generous offering of part of the CCD photometry data.

I appreciate all of the graduate students in the Astronomy group, especially Dave Patton for his help on all aspects of my school life and John Ouellet and Luc Simard for their help in using IRAF.

I thank Whittier's family (Sojung, Edie, and Don) for their consistent warm and generous concern. I also thank all members of Thursday-Bible-Study group - Mary and Larry, Heather and Ken, Huegett and Stan, Lorna, Lorane and Victor, Clare and John - for their praying and accompanying on a spiritual journey.

Finally, I would like to extend my warm thanks to my parents, parents-in-law, brother's and sister's families for their deep understanding of my long-standing student life. I want to dedicate this whole work to my father

who passed away in the middle of summer in 1995. My special thanks *must* go to my life-time partner, Eunyoung Lee and gentle son, Victor Ghiseok, for their love.

Chapter 1

Introduction

Open clusters have been used as templates to study the stellar populations in the Galactic disk in order to determine its formation and evolutionary history. Even though high-quality *CCD* (Charge Coupled Device) detectors were introduced $\sim$ 15 years ago, it is only in recent years with the advent of large format CCD's that open cluster research has benefitted from these developments. Because of their relatively sparse and spatially extended populations, open clusters were not suitable targets for small CCD chips. Much of the research on open clusters has focused on searches for variable stars and on finding the oldest open clusters in order to establish whether or not there is continuity between the disk and the halo of the Galaxy. Perhaps the main reason for widespread interest in open clusters at the present time is that they offer the best available constraints on the extent of convective core overshooting in the main-sequence phase – a matter which is hotly debated.

Since stellar radial-velocity accuracies of better than 1 km s^{-1} have been attained at several observatories (Griffin and Gunn, 1974; Latham, 1985; Mayor, 1985; McClure et al., 1985), studies have been undertaken to de-

termine membership and binary frequency in open clusters, as well as to estimate cluster velocity dispersions. With the information on both the membership and the binary stars in those clusters, constraints on stellar evolution, such as the effect of overshooting, can be improved. From the extensive observations of the red giants in open clusters of various ages, typical spectroscopic-binary frequencies in open clusters range from 25% to 50% (Mermilliod and Mayor 1989, 1990; Mermilliod et al. 1995, 1996, 1997). Abt and Willmarth (1996) note that the frequency of binaries changes in open clusters whose ages range from 1×10^6 to 5×10^8 year, in the sense of increasing with age.

The velocity dispersion of the cluster giants is usually ≤ 1 km s^{-1}, which is consistent with simple virial-theorem estimates, so that it is difficult to study the dynamics of open clusters based on observations with a precision $\sim$1 km s^{-1}.

1.1 Overview of previous studies for NGC 7789

The open cluster NGC 7789 [$\alpha(1950) = 23^h54^m.5$, $\delta(1950) = +56°\ 27'$; $l = 115°.49$, $b = -5°.36$] has been the subject of numerous observational and theoretical studies since Burbidge and Sandage (1958) obtained photoelectric and photographic UBV photometry for about 700 stars within $\sim 450''$ of the cluster center. Their color-magnitude diagram (CMD), which reached as faint as $V = 16.3$ ($\sim$ 2.5 mag below the top of its main sequence), shows a well-defined and extended red-giant branch (RGB), a prominent "clump" of core He-burning stars, many blue stragglers, and a main sequence whose top end bends significantly to the red. Although the foreground reddening

is fairly high, with estimates ranging from $E(B-V) = 0.23$ (Arp, 1962) to 0.32 (Strom and Strom, 1970), it appears to be reasonably uniform across the face of the cluster, judging from the tightness of the observed main sequence in, especially, the recent CCD CMD by Jahn et al. (1995). As indicated in Table 1.1, which also summarizes the available $E(B-V)$ and distance determinations, the metallicity of NGC 7789 appears to be slightly less than solar. It is worth mentioning that giants in NGC 7789 appear to have unusually high Li abundances (Pilachowski, 1986) but unusally low carbon isotope ratios (Sneden and Pilachowski, 1986; Gilroy, 1989) compared with their measured values in field giants.

An extensive proper-motion membership analysis of NGC 7789 was carried out by McNamara and Solomon (1981), who identified 679 probable members brighter than $B \approx 15.5$ ($M_V \sim 2.1$). Radial-velocity measurements by Thogerson et al. (1993), Scott et al. (1995), and Gim et al. (1998) have pretty well established which of the giants are cluster members. In addition, there have been many investigations to ascertain the membership status of the blue straggler candidates — using proper motions (Pendl, 1975; McNamara, 1980), radial velocities (Strom and Strom, 1970; Stryker and Hrivnak, 1984; Drilling and Schönberner, 1987; Manteiga et al., 1989; Milone and Latham, 1994), or polarization data (Breger, 1982). We review the results of all of these investigations in chapter 3.

The fact that NGC 7789 is a very populous cluster gives it considerable potential to test stellar models (simply because its principal photometric sequences on the CMD are very well defined). The curvature of the upper main-sequence and the lack of significant numbers of subgiants is suggestive

Table 1.1: Reddening and metallicity of NGC 7789

E(B−V)	[Fe/H]	$(m-M)_0$	Method	Ref.
0.28		11.36±0.2	*UBV* Photometry	1
0.23			*UBV* Photometry	2
0.32		11.0±0.15	Spectral Type and *ubvy*	3
0.31±0.03	−0.35±0.10	11.37±0.3	*UBV* and *uvby*	4
	−0.1±0.2		spectroscopy (6 giants)	5
0.26	−0.2	11.5	*UBViyz* (19 giants)	6
0.24±0.01	solar comp.	11.5	*DDO* and *UBV* (22 giants)	7
0.22	−0.35		*DDO* and *UBV* (19 giants)	8
	−0.05[a]		Washington system (3 giants)	9
0.32±0.03		11.3±0.02	CCD	10
	−0.26±0.06		Spectroscopy	11

[a]Reported as [A/H]

References

(1) Burbidge and Sandage (1958); (2) Arp (1962); (3) Strom and Strom (1970);
(4) Twarog and Tyson (1985); (5) Pilachowski (1985); (6) Jannens and Helfer (1975);
(7) Janes (1977); (8) Clariá (1979); (9) Canterna et al. (1986);
(10) Martinez Roger et al. (1994); (11) Friel and Janes (1993)

of convective core overshooting (Mazzei and Pigatto, 1988), though Martinez Roger et al. (1994) have argued in favor of classical, non-overshooting models. However, none of the attempts (to date) to fit isochrones to the observed CMD are very convincing. On the one hand, Mazzei and Pigatto conclude that the age of NGC 7789 is 1.1 Gyr, but the isochrone for that age seems too bright in the vicinity of the turnoff and it fails to reproduce the cluster's extended RGB. On the other hand, the non-overshooting isochrones employed by Martinez Roger et al. have a morphology in the vicinity of the turnoff that is not at all like that observed. Even though they find a similar age (1.2 Gyr), their adopted distance modulus differs from the value assumed by Mazzei and Pigatto by nearly 0.5 mag.

On the observational side, too, further work is warranted. For no more than a small fraction of the cluster has a CMD been constructed, and the best available CMD for NGC 7789 (Jahn et al., 1995) extends only to $V \approx 20$ ($M_V \sim 5.5$).

1.2 Current Research

Much more extensive photometric coverage could be expected to reveal more giants, perhaps extending the RGB to redder colors, and a deeper survey would delineate the lower main sequence to much fainter magnitudes, thereby offering stronger constraints on stellar models and facilitating comparisons with the CMDs of other clusters having similar metallicities. It is for these reasons, and to revisit the question as to whether models with, or without, convective overshooting are better able to explain the observations, that we have undertaken this investigation.

This study combines large area-coverage V and I CCD photometry with radial velocities for clump stars and more luminous giants, from which we can determine the membership and the spectroscopic binary frequency. However, the data are not extensive enough to obtain orbital elements for the proposed binary stars.

Our photometric and radial velocity data and their reductions are presented in chapter 2, and analysed in chapter 3, and a brief summary of the main results of this investigation are given in chapter 4.

Chapter 2

Observations and Data Reduction

This project uses observational data that were obtained by D. Zurek in 1993 and by myself in 1995 with different CCD detectors but using the same telescope. All data were reduced by the stand-alone DAOPHOT, ALLSTAR and ALLFRAME codes with various auxiliary programs developed by Dr. Stetson. On the other hand, the cross-correlation radial-velocity spectrometer (RVS) has been used to get the radial velocities for most of the giant stars in NGC 7789 in 1995 and 1996, extending the time base line for most previously observed stars, with some of the DAO observations dating back to 1979.

2.1 CCD photometric observations

Observations for this project were made at the f/5 modified Newtonian focus of the Dominion Astrophysical Observatory (DAO) 1.8 m Plaskett telescope, by Zurek with the Tek-2 CCD on the nights of 1993 October 10/11, 15/16, and December 16/17, and by myself with the SITe-1 CCD on 1995 October

31/November 1, November 1/2, December 5/6, 6/7, and 8/9. Each detector contains 1024 × 1024 pixels at a scale of 0.53 arcsec per pixel, yielding a 9 × 9 arcmin^2 image size. The gain and readout noise were 4.0 e^-/ADU and 11 e^- for Tek-2 CCD and 4.7 e^-/ADU and 13 e^- for the SITe-1 CCD detector. A Johnson V, I filter set was used.

Table 2.1 contains an observational record for NGC 7789, and Figs. 2.1 and 2.2 show the observational area for each frame. We used a total of 316 frames, among which 66 (33 frames each in V and I) were exposed for 600 s, 74 (37 frames each in V and I) for 60 s and 76 (38 frames each in V and I) for 6 s. An additional ten frames had 10 s exposures in V. There was considerable frame-to-frame overlap among adjacent fields. The diameter of the total cluster area covered was roughly 35 arcmin. The full-width at half-maximum (FWHM) of the stellar image cores ranges from 2.″2 to 3.″2 except those taken on 1995 December 7, for which the FWHM is about 4.″0 because telescope tracking problems and strong winds resulted in elongated star images on some frames. Primary standard stars were taken from Landolt's *UBVRI* standard stars (Landolt, 1992; Stetson, 1997) and also from stars in the globular cluster NGC 7006 (Davis, 1992; Stetson, 1997) and the open cluster M 67 (Montgomery et al., 1993). Table 2.2 contains details of the CCD frames for standard stars.

Table 2.1: Journal of NGC 7789 Observations

UT[a]	R[b]	F[c]	Int.[d] (sec)	X[e]	UT[a]	R[b]	F[c]	Int.[d] (sec)	X[e]	UT[a]	R[b]	F[c]	Int.[d] (sec)	X[e]
11 OCT 1993														
5:15	A	I	600	1.030	6:10		V	10	1.016	6:59		V	60	1.011
5:33		I	60	1.030	6:12		I	600	1.015	7:26		V	10	1.015
5:35		I	3	1.030	6:24		I	60	1.013	7:29	D	V	60	1.016
5:37		V	600	1.028	6:26		I	3	1.012	7:34		I	60	1.017
5:49		V	60	1.023	6:30	C	I	600	1.012	7:42		I	3	1.019
5:52		V	10	1.023	6:42		I	60	1.011	7:43		I	600	1.020
5:56	B	V	600	1.020	6:44		I	3	1.011	7:55		V	600	1.025
6: 7		V	60	1.017	6:46		V	600	1.010	3:46		V	10	1.109
16 Dec 1993														
3:46	A	V	10	1.109	4:58	C	V	10	1.041	6: 9	B	V	10	1.012
3:50		V	60	1.105	5: 0		V	60	1.040	6:17		V	10	1.011
3:52		V	600	1.102	5: 3		V	600	1.038	6:19		V	10	1.011
4: 4		I	600	1.088	5:15		I	600	1.025	6:21		V	60	1.010
4:16		I	60	1.075	5:27		I	60	1.025	6:24		V	600	1.010
4:20		I	3	1.069	5:30		I	3	1.023	6:36		I	600	1.010
4:23	B	I	3	1.069	5:34	D	I	3	1.022	6:48		I	60	1.011
4:25		I	60	1.068	5:36		I	60	1.021	6:51		I	3	1.012
4:27		I	600	1.065	5:39		I	600	1.020	6:53	F	I	3	1.012
4:40		V	600	1.054	5:50		V	600	1.015	6:55		I	60	1.013
4:52		V	60	1.044	6: 2		V	60	1.013	6:58		I	600	1.013
4:55		V	10	1.042	6: 6		V	10	1.012	2:26		V	60	1.010
17 DEC 1993														
2:26	E	V	60	1.010	3:14		V	60	1.018	3:51		I	600	1.035
2:29		V	600	1.010	3:16		V	600	1.019	4: 4	H	I	30	1.043
2:42		I	30	1.011	3:29	G	V	60	1.024	4: 7		I	600	1.045
2:45		I	600	1.011	3:32		V	600	1.025	4:19		V	30	1.055
2:59	F	I	30	1.014	3:45		I	30	1.032	4:21		V	60	1.057
3: 2		I	600	1.014	3:47		I	30	1.033	4:24		V	600	1.060

Table 2.1: *Continued*

UT[a]	R[b]	F[c]	Int.[d] (sec)	X[e]	UT[a]	R[b]	F[c]	Int.[d] (sec)	X[e]	UT[a]	R[b]	F[c]	Int.[d] (sec)	X[e]
1 NOV 1995														
3:44	A	V	10	1.049	5:32		V	600	1.010	8:44		I	60	1.155
3:47		V	60	1.047	5:44		I	600	1.011	8:47		I	6	1.159
3:49		V	600	1.046	6: 7		I	60	1.015	9:47	F	I	3	1.283
4: 1		I	600	1.038	6:17		I	6	1.018	9:48		I	6	1.285
4:17		I	60	1.029	6:19		I	3	1.019	9:50		I	60	1.288
4:21		I	6	1.027	7:26	D	I	2	1.060	9:52		I	600	1.295
4:27		I	3	1.024	7:28		I	6	1.062	10: 4		V	600	1.324
4:32	B	I	3	1.022	7:32		I	60	1.066	10:22		V	60	1.372
4:35		I	6	1.020	7:39		I	600	1.072	10:24		V	10	1.380
4:37		I	60	1.020	7:55		V	600	1.089	10:28	G	V	10	1.392
4:40		I	600	1.016	8: 9		V	60	1.106	10:30		V	60	1.399
5: 2		V	600	1.013	8:12		V	10	1.109	10:33		V	600	1.406
5:18		V	60	1.011	8:16	E	V	10	1.114	10:45		I	600	1.444
5:22		V	10	1.010	8:18		V	60	1.116	10:56		I	60	1.484
5:27	C	V	10	1.010	8:21		V	600	1.120	10:59		I	6	1.492
5:29		V	60	1.010	8:32		I	600	1.136	11: 1		I	3	1.498
2 NOV 1995														
3:51	A	I	3	1.041	6:25		V	6	1.023	9:25		I	6	1.240
3:58		I	6	1.037	7: 6	D	V	6	1.048	9:26		I	3	1.243
4: 1		I	60	1.034	7: 8		V	60	1.049	9:34	G	I	3	1.265
4: 4		I	600	1.032	7:10		V	600	1.051	9:36		I	6	1.267
4:17		V	600	1.026	7:22		I	600	1.061	9:38		I	60	1.271
4:29		V	60	1.021	7:44		I	60	1.081	9:40		I	600	1.278
4:32		V	6	1.019	7:47		I	6	1.086	9:52		V	600	1.306
4:34	B	V	6	1.019	7:51		I	3	1.089	10: 4		V	60	1.337
4:38		V	60	1.018	8: 0	E	I	3	1.099	10: 7		V	6	1.344
4:52		V	600	1.017	8: 1		I	6	1.101	10:13	H	V	6	1.359
5:30		I	600	1.009	8: 3		I	60	1.102	10:15		V	60	1.364
5:43		I	60	1.011	8:19		I	600	1.123	10:18		V	60	1.372
5:45		I	6	1.011	8:30		V	600	1.139	10:21		V	6	1.379
5:50		I	3	1.012	8:44		V	60	1.162	10:24	I	V	6	1.386

Table 2.1: *Continued*

UT[a]	R[b]	F[c]	Int.[d] (sec)	X[e]	UT[a]	R[b]	F[c]	Int.[d] (sec)	X[e]	UT[a]	R[b]	F[c]	Int.[d] (sec)	X[e]
5:53	C	I	3	1.012	8:46		V	6	1.165	10:26		V	60	1.393
5:55		I	6	1.013	8:54	F	V	6	1.181	10:29		I	60	1.402
5:56		I	60	1.013	8:56		V	60	1.184	10:31		I	6	1.409
5:59		I	600	1.014	8:59		V	600	1.190	10:35		I	2	1.421
6:11		V	600	1.017	9:10		I	600	1.211	4:22		I	3	1.028
6:23		V	60	1.022	9:22		I	60	1.235	4:27		I	60	1.030
6 DEC 1995														
4:22	A	I	3	1.028	5:40	C	I	3	1.091	6:56	E	I	3	1.203
4:27		I	60	1.030	5:42		I	6	1.093	6:57		I	6	1.205
4:30		I	6	1.032	5:44		I	60	1.094	7: 0		I	60	1.211
4:55		V	60	1.049	6:10		V	60	1.128	7:25		V	60	1.265
4:58		V	6	1.051	6:14		V	6	1.135	7:30		V	6	1.274
5: 4	B	V	6	1.056	6:18	D	V	6	1.140	8:41		I	3	1.484
5: 7		V	60	1.058	6:22		V	60	1.145	8:41	F	I	6	1.486
5:33		I	60	1.084	6:48		I	60	1.189	8:43		I	60	1.492
5:36		I	6	1.087	6:50		I	6	1.193	9:10		V	60	1.593
5:38		I	3	1.088	6:52		I	3	1.196	2:42		V	6	1.012
7 DEC 1995														
2:42	A	V	6	1.012	4:38		I	60	1.040	7: 2		I	6	1.227
2:44		V	10	1.011	5: 3		V	60	1.060	7: 3		I	3	1.231
2:46		V	60	1.011	5: 6		V	10	1.062	7: 7	H	I	3	1.241
3:12		I	60	1.010	5: 8		V	6	1.064	7: 9		I	6	1.246
3:15		I	6	1.010	5:11	E	V	6	1.066	7:10		I	60	1.249
3:16		I	3	1.010	5:12		V	10	1.067	7:36		V	60	1.308
3:19	B	I	3	1.010	5:14		V	60	1.068	7:38		V	10	1.315
3:20		I	6	1.011	5:40		I	60	1.097	7:40		V	6	1.319
3:22		I	60	1.011	5:43		I	6	1.100	7:47	I	V	10	1.338
3:49		V	60	1.016	5:44		I	3	1.102	7:52		V	60	1.351
3:51		V	10	1.017	5:55	F	I	3	1.117	8:19		I	60	1.430
3:53		V	6	1.018	5:56		I	6	1.119	8:21		I	6	1.442
3:56	C	V	6	1.019	5:57		I	60	1.120	8:23		I	3	1.445
3:58		V	10	1.019	6:23		V	60	1.159	8:30	J	I	6	1.468

Table 2.1: *Continued*

UT[a]	R[b]	F[c]	Int.[d] (sec)	X[e]	UT[a]	R[b]	F[c]	Int.[d] (sec)	X[e]	UT[a]	R[b]	F[c]	Int.[d] (sec)	X[e]
4: 1		V	60	1.021	6:26		V	10	1.163	8:32		I	60	1.474
4:27		I	60	1.034	6:27		V	6	1.166	8:58		V	60	1.568
4:30		I	6	1.035	6:32	G	V	6	1.170	9: 0		V	10	1.577
4:32		I	3	1.036	6:33		V	10	1.173	9: 2		V	6	1.584
4:34	D	I	3	1.038	6:34		V	60	1.175	2:12		V	6	1.017
4:36		I	6	1.039	6:59		I	60	1.223	2:14		V	10	1.016
9 DEC 1995														
2:12	G	V	6	1.017	5:10	I	I	3	1.073	7:19	K	I	3	1.290
2:14		V	10	1.016	5:11		I	6	1.074	7:21		I	6	1.295
2:16		V	60	1.016	5:15		I	60	1.078	7:23		I	60	1.301
2:18		V	600	1.015	5:18		I	600	1.081	7:26		I	600	1.307
2:30		I	600	1.012	5:30		V	600	1.095	7:38		V	600	1.338
2:42		I	60	1.011	5:42		V	60	1.110	7:50		V	60	1.371
2:45		I	3	1.010	5:47		V	10	1.116	7:52		V	10	1.378
2:47		I	6	1.010	5:48		V	6	1.118	7:54		V	6	1.384
4:31	H	V	6	1.041	6:40	J	V	6	1.205	7:58	L	V	6	1.390
4:32		V	10	1.042	6:42		V	10	1.209	8: 0		V	10	1.400
4:34		V	60	1.043	6:44		V	60	1.213	8: 2		V	60	1.407
4:37		V	600	1.045	6:46		V	600	1.218	8: 5		V	600	1.430
4:49		I	600	1.054	6:58		I	600	1.242	8:17		I	600	1.453
5: 0		I	60	1.064	7:10		I	60	1.268	8:32		I	6	1.506
5: 4		I	6	1.068	7:13		I	6	1.275	8:35		I	3	1.515
5: 6		I	3	1.070	7:15		I	3	1.280					

[a]Universal Time
[b]Regions marked on Figs. 2.1 and 2.2
[c]Filters
[d]Exposure time
[e]Air mass

Table 2.2: Journal of Standard Star Observations

Name	DATE	UT	Filter	Int. (sec)	Air mass
NGC7006	1/NOV/95	2:17	I	10	1.183
NGC7006	1/NOV/95	2:25	I	120	1.184
NGC7006	1/NOV/95	2:30	V	50	1.184
NGC7006	1/NOV/95	2:32	V	150	1.184
NGC7006	1/NOV/95	2:39	V	300	1.184
PG0231	1/NOV/95	8:54	I	60	1.401
PG0231	1/NOV/95	8:57	I	100	1.405
PG0231	1/NOV/95	9: 1	I	100	1.410
PG0231	1/NOV/95	9:15	V	200	1.433
SA95	1/NOV/95	11:28	V	500	1.758
SA95	1/NOV/95	11:51	I	200	1.884
SA98-670	1/NOV/95	12:30	V	500	1.518
SA98-670	1/NOV/95	12:47	V	300	1.527
SA98-670	1/NOV/95	13: 3	I	60	1.541
SA98-626	1/NOV/95	13: 6	I	60	1.547
SA98-626	1/NOV/95	13: 9	I	40	1.551
SA98-626	1/NOV/95	13:12	I	30	1.555
SA98-626	1/NOV/95	13:18	V	120	1.565
NGC7006	2/NOV/95	3:15	V	300	1.201
NGC7006	2/NOV/95	3:36	I	120	1.223
SA95	2/NOV/95	11:11	I	200	1.708
SA95	2/NOV/95	11:20	I	150	1.740
SA95	2/NOV/95	11:35	V	400	1.817
SA98-670	2/NOV/95	12:21	V	60	1.518
SA98-670	2/NOV/95	12:24	V	30	1.518
SA98-670	2/NOV/95	12:32	I	5	1.520
SA98-670	2/NOV/95	12:34	I	10	1.521
SA98-626	2/NOV/95	12:37	I	30	1.521
SA98-626	2/NOV/95	12:41	I	20	1.523
SA98-626	2/NOV/95	12:49	V	80	1.532
SA98-626	2/NOV/95	12:53	V	40	1.536
NGC7006	6/DEC/95	2:23	I	120	1.331
NGC7006	6/DEC/95	2:28	I	150	1.346

Table 2.2: *Continued*

Name	DATE	UT	Filter	Int. (sec)	Air mass
NGC7006	6/DEC/95	2:57	V	300	1.437
NGC7006	6/DEC/95	3: 4	V	150	1.463
PG0231	6/DEC/95	3:56	V	150	1.534
PG0231	6/DEC/95	4: 5	I	60	1.509
SA98-670	6/DEC/95	9:49	V	200	1.522
SA98-670	6/DEC/95	9:54	V	100	1.520
SA98-670	6/DEC/95	9:57	V	50	1.518
SA98-670	6/DEC/95	10: 4	I	10	1.517
SA98-590	6/DEC/95	10:10	I	10	1.519
SA98-590	6/DEC/95	10:12	I	5	1.519
SA98-590	6/DEC/95	10:16	V	40	1.520
SA98-590	6/DEC/95	10:19	V	30	1.521
M67	6/DEC/95	11:22	I	3	1.264
M67	6/DEC/95	11:25	I	1	1.262
M67	6/DEC/95	11:26	I	6	1.261
M67	6/DEC/95	11:28	I	30	1.259
M67	6/DEC/95	11:31	V	3	1.257
M67	6/DEC/95	11:33	V	6	1.256
M67	6/DEC/95	11:34	V	30	1.255
M67	6/DEC/95	11:37	V	60	1.254
NGC7006	9/DEC/95	2:58	I	120	1.497
NGC7006	9/DEC/95	3: 6	V	300	1.536
PG0231	9/DEC/95	3:41	V	60	1.538
PG0231	9/DEC/95	3:45	V	180	1.524
PG0231	9/DEC/95	3:51	I	150	1.508
PG0220	9/DEC/95	3:57	I	150	1.294
PG0220	9/DEC/95	4:16	V	500	1.265
PG0231	9/DEC/95	5:54	V	180	1.376
PG0231	9/DEC/95	6: 3	V	180	1.381
PG0231	9/DEC/95	6: 8	I	150	1.385
PG0220	9/DEC/95	6:14	I	300	1.244
PG0220	9/DEC/95	6:21	V	500	1.251

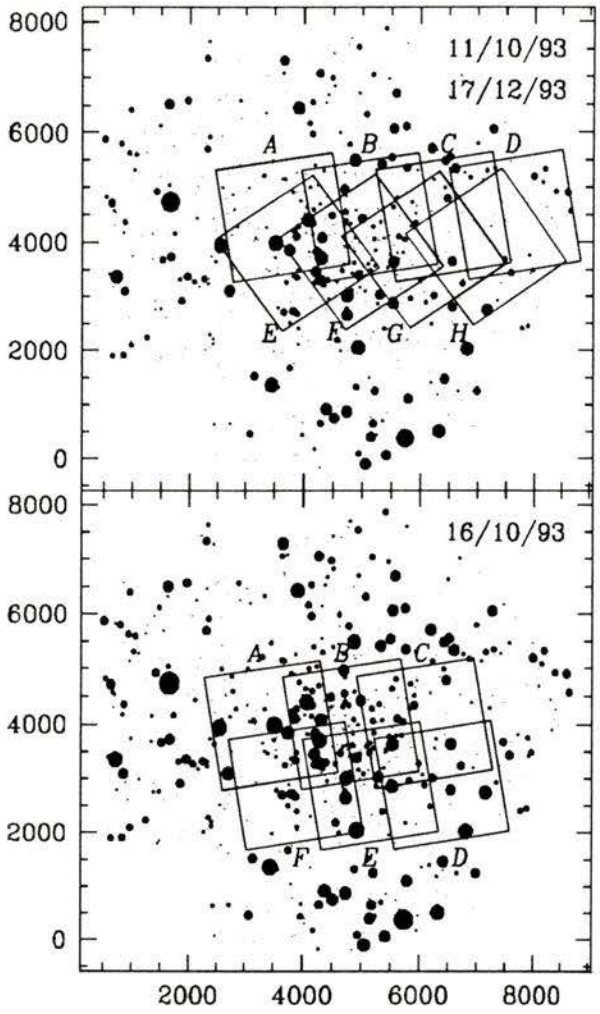

Figure 2.1: The area observed in the vicinity of NGC 7789. For the sake of clarity, only stars brighter than the faintest clump star ($V \sim 13.4$) are plotted. Units on the horizontal and vertical axes are pixels, where 2048 pixels correspond to 9.'2. The center of each panel (4628, 3873) is nearly identical with the cluster center. The date of observation is shown in the upper right of each panel. East is to the right and North is to the top.

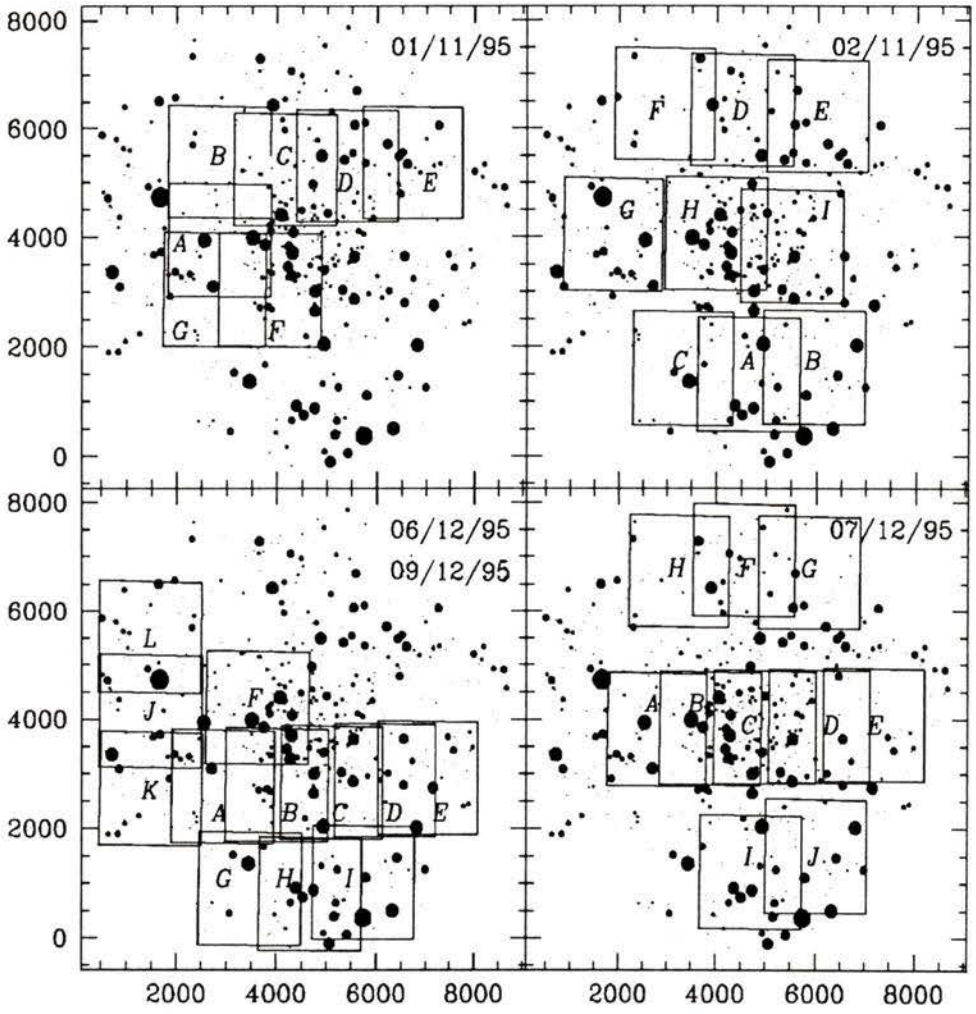

Figure 2.2: Same as Fig. 2.1

2.1.1 Photometry

All of the CCD image frames were subjected to two preprocessing steps, bias subtraction and flat fielding, in order to remove the instrumental signature; this was done with IRAF[1]. After the raw images from a given night were corrected for the floating bias level based on the overscan region and after they were properly trimmed, about 10 bias frames were median-combined into one bias-pattern frame, which was then subtracted from the raw images. During the various observing runs, mostly dusk and dawn sky flat frames were recorded, but on one night flat-field images were obtained by observing the undersides of clouds. All frames were divided by the median-combined flat frames for each filter on each night to remove pixel-to-pixel sensitivity variations.

All photometric reductions and analysis following the above preprocessing were accomplished by automatic profile-fitting techniques: DAOPHOT, ALLSTAR (Stetson, 1987) and ALLFRAME (Stetson, 1994). Initial star lists and instrumental magnitudes for each frame were obtained from the general procedure with DAOPHOT and ALLSTAR, for which detailed explanations are given in the *DAOPHOT II USER's Manual* and by Stetson (1987). The first reduction steps on all frames are to identify star-like images with intensities over a certain multiple (here four times) of the background sky noise, to obtain approximate magnitudes for those stars, to make a model point-spread function (PSF) for each frame from stars which are bright and well-isolated, and finally to obtain more accurate positions and magnitudes

[1]IRAF is distributed by the National Optical Astronomy Observatories, which are operated by the Association of Universities for Research in Astronomy, Inc., under contract with the National Science Foundation

of all stars by least-squares fitting of the PSFs. The most time-consuming steps are the selection of stars for making the PSFs, and the identification of faint stars which were not detected by the automatic scheme due to their being confused with nearby brighter stars. The approximate fitting function for the PSF was decided automatically for each frame (see Table 2.3) as one of six different analytic models; tabulated sub-pixel corrections from the analytic model to the true empirical PSF were allowed to vary linearly with position in the frames.

Table 2.3: Number of Frames Using Each PSF Function

PSF	1993			1995				
Function	11Oct	16Oct	17Dec	1Nov	2Nov	6Dec	7Dec	9Dec
Gaussian	11	16	0	6	0	0	0	1
Lorentz	0	2	0	0	0	0	0	0
Moffat15	0	0	0	0	0	2	1	0
Moffat25	0	1	8	3	1	0	8	0
Penny1	7	11	6	13	19	7	15	18
Penny2	5	5	4	33	32	19	34	28

The next step of the reduction procedure is a challenging one in this work. One comprehensive star list with a unique coordinate system is required before running ALLFRAME. However, as shown in the Figures 2.1 and 2.2, it is not easy to match up all star lists from all frames, which are partially overlapped but greatly spread out in order to have greater areal coverage. A set of plates of NGC 7789 from the Mount Wilson 100-inch Hooker telescope was used to provide a single coordinate system spanning the full area of the cluster, to which the CCD images could be individually

referred. The program DAOMASTER was used to estimate the individual geometric transformation equations relating the coordinate systems of the various frames to make the composite starlist for input to ALLFRAME.

The philosophy and usage of ALLFRAME are discussed by Stetson (1994). ALLFRAME derives a self-consistent set of positions and magnitudes for all detected star-like objects in an area of sky by using the geometric and photometric information from all images of a given field.

2.1.2 Aperture Corrections

Profile-fitting photometry yields relative magnitude measurements within a given field; the zero point of this magnitude system is a variable quantity related to the flux volume of the model PSF, which is not necessarily specified with high accuracy. An additive correction to place the relative magnitudes derived from a given image on a repeatable absolute scale can be determined by synthetic-aperture measurements of a number of selected, bright, isolated stars in the field (for a comprehensive explanation, see Stetson 1990). In this project the concentric-aperture photometry was based on the same stars that were used for defining the PSFs, employing apertures ranging from small (3 pixels) to large radii (25 pixels) on copies of the frames where all stars except the selected stars had been digitally subtracted.

2.1.3 Standardisation

We have chosen Landolt's (1992) observations as the basis of our standard system. However, to improve the internal homogeneity and precision of our results, we have combined our own measurements of Landolt's stars over the

course of 15 years with his published data, producing refined magnitudes and colors which retain the overall zero points and color scales of the Landolt system, but with better precision and internal consistency. Two other primary standard fields are used in our calibrations: 28 stars in the open cluster M67 (Montgomery et al., 1993) and 124 stars in the globular cluster NGC 7006 (Davis, 1992; Stetson, 1997). Both photometric systems are also closely tied to Landolt's.

Instrumental magnitudes for all detected stars were transformed to the standard V and I magnitudes using the relations

$$v = V + a_0 + a_1(V - I) + a_2(X - 1.25) + a_3T, \tag{2.1}$$

$$i = I + b_0 + b_1(V - I) + b_2(X - 1.25) + b_3T, \tag{2.2}$$

where v, i are the instrumental magnitudes in the V and I filters, respectively, and X is the airmass and T is the time of the observation (the terms in T allow for the zero-order effects of any extinction variations during the night); the a_i, b_i are unknown transformation coefficients. For three photometric nights in 1995, all the above coefficients were determined from the primary standard stars; Table 2.4 contains our derived values for the color-dependent coefficients a_1 and b_1 and Table 2.5 for the other corresponding values. We defined a local standard sequence in the field of NGC 7789 based on the above transformations for the photometric nights. These local stars were then added to the standard list to improve the photometric tie-in among the three photometric nights, and also to determine the photometric zero points for individual frames obtained on non-photometric nights. As shown in Tables 2.1 and 2.2, the standard stars were mostly observed at airmasses

larger than 1.2, while for many of the NGC 7789 frames the airmasses were less than 1.1 and for others the airmasses were much larger.

Table 2.4: Color-dependent coefficients (Mean values)

Date	Detector	V		I	
		a_1	σ	b_1	σ
1993	Tek-2	−0.0134	0.0042	−0.0405	0.0063
1995	SITe-1	−0.0108	0.0013	−0.0349	0.0026

Table 2.5: Color-independent coefficients (Individual values)

Date	V				I			
	a_2	σ	a_3	σ	b_2	σ	b_3	σ
1/11/95	0.1840	0.0039	−0.0072	0.0002	0.0787	0.0068	−0.0091	0.0004
2/11/95	0.1790	0.0048	−0.0059	0.0003	0.0642	0.0049	−0.0114	0.0003
6/12/95	0.2118	0.0017	−0.0052	0.0001	0.0713	0.0028	−0.0068	0.0001

Figure 2.3 shows the residuals (in the sense of *present* − *standard*) in V and $(V-I)$ as functions of apparent magnitude and color for the primary standard stars. The offset and the standard error of the mean offset in V and $(V-I)$ based on 274 stars are -0.0024 ± 0.0009; s.d. $= 0.025$ and -0.0019 ± 0.0014; s.d. $= 0.030$, respectively.

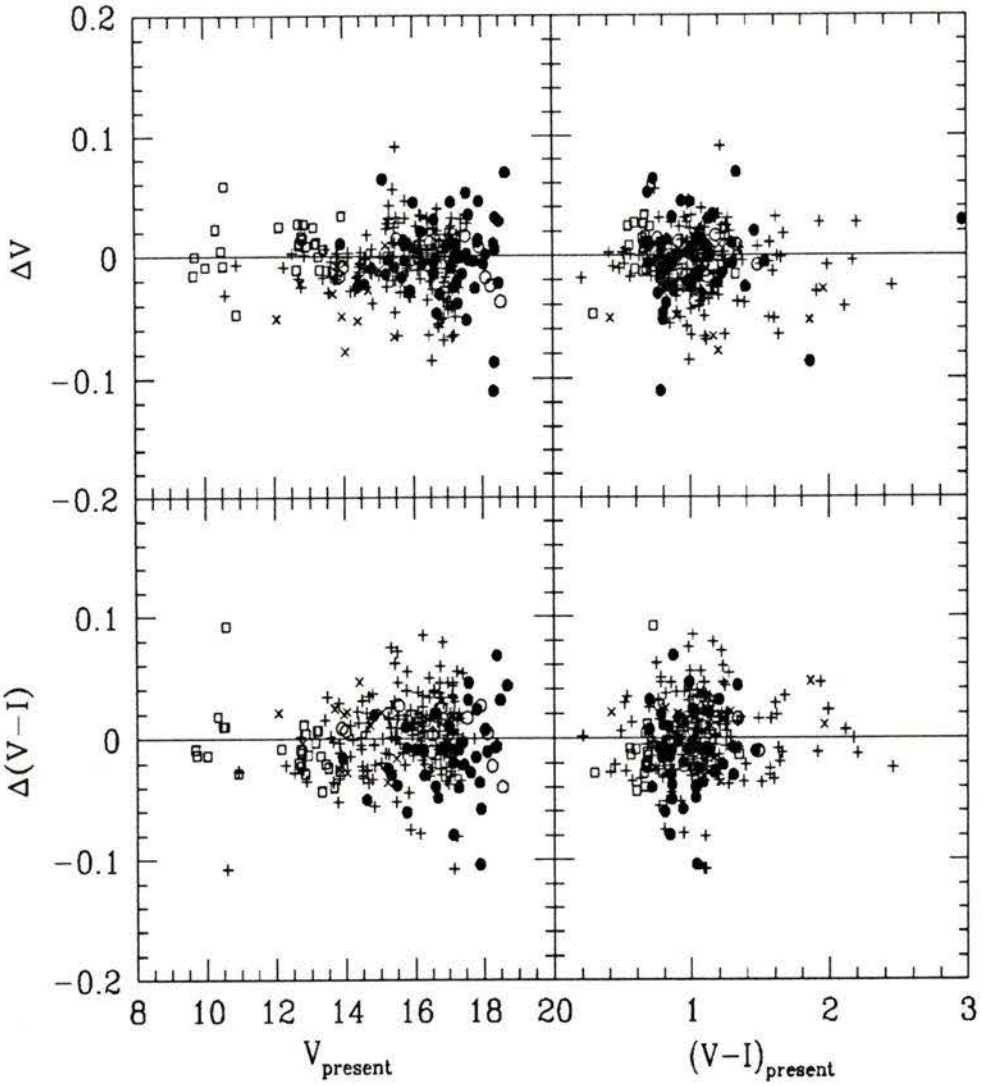

Figure 2.3: Residuals (in the sense of "present" − "standard") in V and $V - I$ as functions of apparent magnitude and color for the primary standard stars. *Crosses*: Landolt (1992) standards; *pluses*: Landolt stars (Stetson 1997); *open squares*: M67 stars (Montgometry et al. 1993); *solid circles*: NGC 7006 stars (Davis 1992); and *open circles*: NGC 7006 stars (Stetson 1997).

2.1.4 Comparison with other photometry for NGC7789

In order to check the reliability of the calibration, our V magnitudes for NGC 7789 stars were compared with six previous sets of photoelectric UBV photometry (Burbidge and Sandage, 1958; Janes, 1977; Breger, 1982; Coleman, 1982; Jennens and Helfer, 1975; Breger and Wheeler, 1980), two sets of photographic BV photometry (Burbidge and Sandage, 1958; McNamara, 1980), and CCD photometry in BV by Jahn et al (1995). The comparisons were made only for V because no I-band photometry has previously been published. The differences in V magnitude, in the sense of (*present – published*), as functions of V magnitude and $(V - I)$ color are shown in Figs. 2.4, 2.5 and 2.6. Table 2.6 shows the mean offset and slope in the three plots.

The mean and standard deviation of the magnitude residuals indicate that the offset between our CCD photometry and the previous photoelectric photometry in Fig. 2.4 is negligible, +0.003 mag (30 stars) and −0.006 mag (18 stars), but the standard deviations, 0.035 mag and 0.033 mag, are appreciable. The comparison with previous photographic photometry (Fig. 2.5) shows significant offsets: $\Delta V = 0.053$ mag (284 stars) and 0.018 mag (62 stars) with standard deviations of 0.045 mag and 0.061 mag, respectively. In addition, a systematic trend in V magnitude with the $(V - I)$ colors was found in comparison with both photoelectric and photographic photometry in the sense that our CCD photometry is brighter than published photometry for the bluer stars, with a slope of 0.032 to 0.068. In contrast, a comparison (Fig. 2.6) with other CCD photometry (Jahn et al., 1995) appears to reveal a slight zero point shift of about 0.021 mag, but no systematic trend with color.

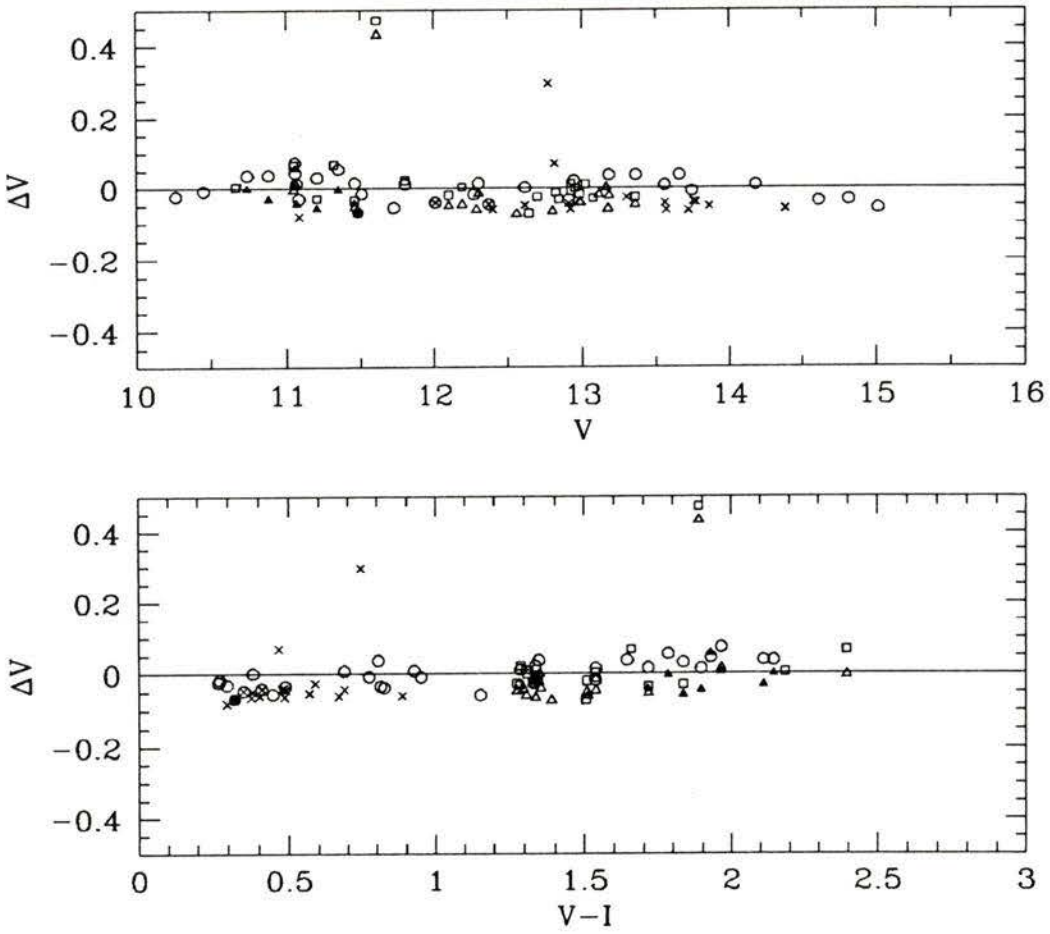

Figure 2.4: V magnitude comparison between our data and several published data sets obtained with photoelectric photometry. *Open circles*: Burbidge and Sandage (1958), *crosses*: Breger (1982), *squares*: Janes (1977), *solid triangles*: Coleman (1982), *open triangles*: Jennens and Helfer (1975), and *solid circles*: Breger and Wheeler (1980). Stars with large differences in the plot are M589 (one from Janes (1977) and the other from Jennens and Helfer (1975)), M467 (Breger, 1982) and M789 (Breger, 1982). In addition, M292 (Breger, 1982) and M864 (Janes, 1977) have $|\Delta V| > 0.5$. V and $V - I$ on the horizontal axes are the magnitude and color from the present study. See Table 2.6 for a statistical summary of these plots.

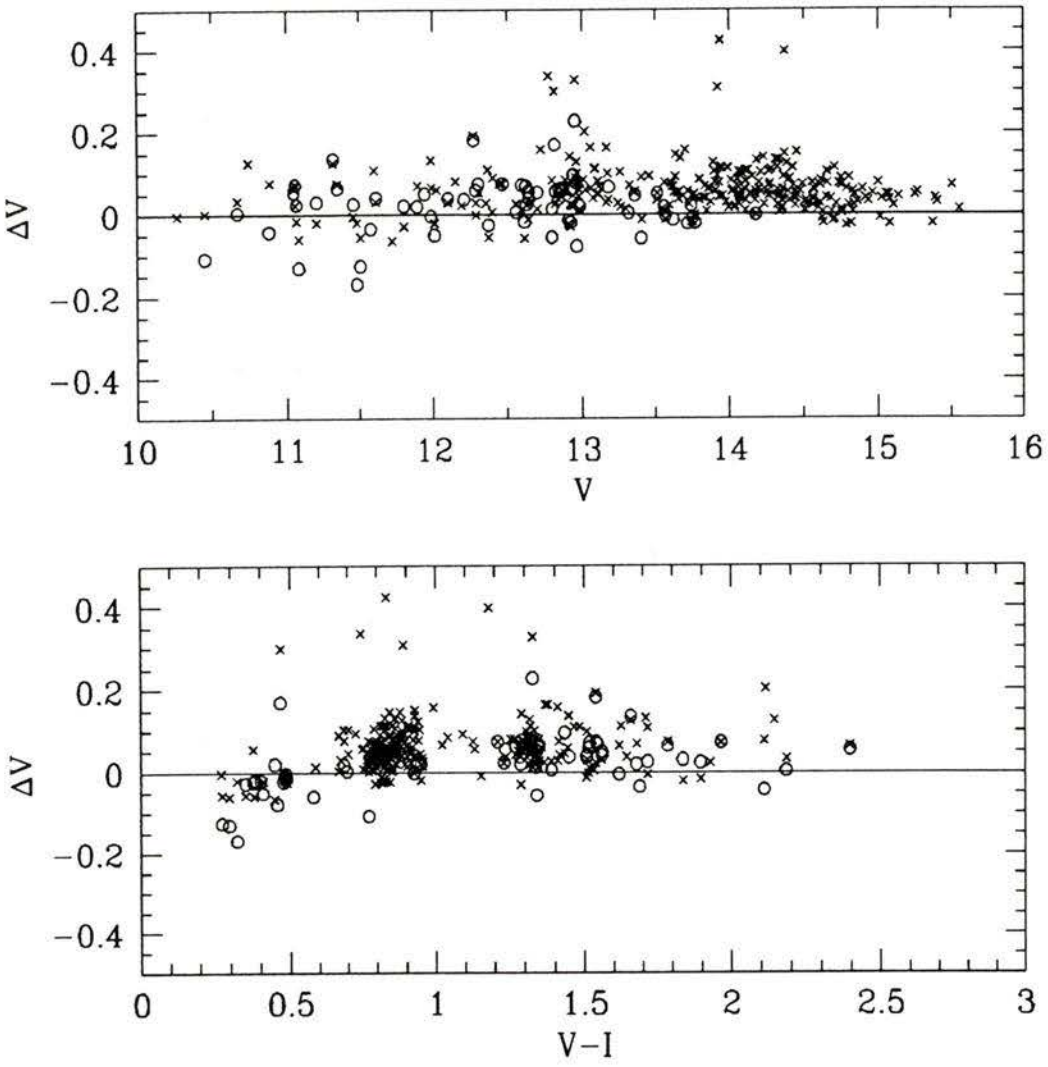

Figure 2.5: Same as Fig. 2.4, but comparing the present data with published photographic photometry. *Crosses*: Burbidge and Sandage (1958), *open circles*: McNamara (1980). Four stars (M589, M1012, M818, and M717) from Burbidge and Sandage (1958) and three stars (M589, M1012, and M1054) from McNamara (1980) have $|\Delta V| > 0.5$. See Table 2.6 for a statistical summary of these plots.

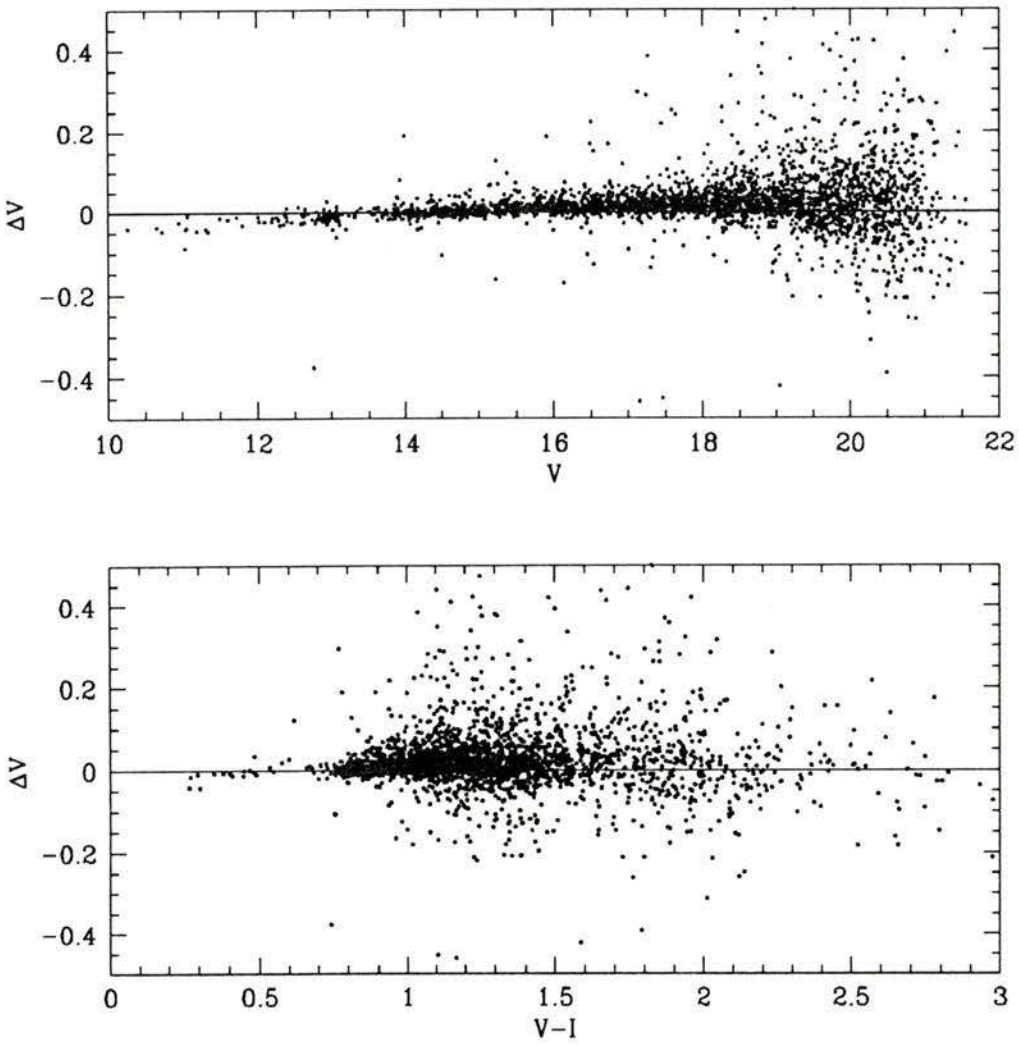

Figure 2.6: Same as Fig. 2.4, but comparing the present data with published CCD photometry (Jahn et al. 1995). The total number of stars in this plot is 3030 including two stars with $|\Delta V| > 0.5$. See Table 2.6 for a statistical summary of these plots.

Table 2.6: Comparison with the Published Photometry

Ref.	No.[a]	ΔV vs. V		ΔV vs. $V-I$	Excluded
		Mean	s.d.	Slope	Stars
photoelectric photometry					
1	30	0.003	0.035	0.041	
2	16	−0.051	0.014	small	M789, M467, M292
3	19	−0.006	0.033	0.041	M589, M864
4	8	−0.016	0.037	small	
5	16	−0.037	0.026	0.048	M589
6	1				
Total	89	-0.017	0.038	0.028	
Photographic photometry					
7	284	0.053	0.045	0.032	11 stars with $\Delta V > 0.3$
8	63	0.018	0.061	0.068	4 stars with $\Delta V > 0.2$
CCD photmetry					
9	3030	0.021	0.071	0.005	

[a]Number of stars compared

References

1: Burbidge and Sandage (1958); 2: Breger (1982); 3: Janes (1977)
4: Coleman (1982); 5: Jennens and Helfer (1975); 6: Breger and Wheeler (1980)
7: Burbidge and Sandage (1958); 8: McNamara (1980); 9: Jahn et al. (1995)

2.2 Radial-velocity observations

Radial-velocity observations for NGC 7789 were initiated by McClure and Hesser in 1979 with the cross-correlation radial-velocity spectrometer (RVS) at the coudé spectrograph of the Dominion Astrophysical Observatory (DAO) 1.2-m telescope. A detailed description of the DAO RVS is given by Fletcher et al. (1982) and McClure et al. (1985). We summarise here some points important to this project.

2.2.1 Overview of RVS

The RVS, following the principle of the Cambridge photoelectric radial-velocity spectrometer (Griffin, 1967), includes a transmissive spectral mask, a Fabry lens and a photomultiplier. Unique designs for the Fabry system and spectrum mask make it possible to observe radial velocities of stars down to $\sim$16.0 B magnitude at the DAO 1.2-m telescope (McClure et al., 1985).

The K star mask used contains 454 stellar and 14 comparison lines, covering the wavelength range from 4332Å to 4765Å and was based on the spectrum of Arcturus. Two image slicers were used for the observations: IS32B and ISRVS. The former has smaller guiding errors at times of good seeing but admits less light.

Comparison observations of a Cd-Ar source were obtained about every 30 - 60 minutes during each night in order to correct the zero point drift, which was usually less than 1 km s^{-1} except for a few nights having a drift of unknown origin up to 3 km s^{-1}. Typically, about 10 radial-velocity standards as well as the twilight sky were observed every night to tie our observations to the IAU system. Cluster star exposure times were from $\sim$15 minutes

to ~30 minutes, depending on the faintness of the stars, seeing and transparency. Scan widths were mostly ~18 km s^{-1} for cluster stars. Normally, this scan range covers over two-thirds of the cross-correlation dip, and the radial velocity is calculated using a parabolic function fit to the dip.

2.2.2 RVS Observations and reductions

The RVS data reduction procedure after observing is straightforward. The comparison velocity is plotted against the universal time (UT) and is subtracted from the stellar velocities for the time of observation. Secondly, a correction is made to the standard velocities of the DAO RVS system using radial-velocity standard values compiled by McClure. These provide improved individual velocities, and agree in the mean with the standard values published by Fletcher et al. (1982). For 30 stars in common the velocity difference (McClure − Fletcher et al.) is -0.013 ± 0.38 (s.d.) km s^{-1}.

From the precision of the measurements, the internal error of the observations is better than 0.4 km s^{-1} for stars brighter than $B = 9.0$ magnitude. Fletcher et al. (1982) and McClure et al. (1985) addressed the fact that the size of the slit entrance and the seeing are two factors affecting random error.

Overall, 597 observations for 112 stars were obtained on 71 nights from 1979 to 1996 (see Table 2.7). The Julian date, radial velocity and internal error for each star are shown in Appendix A (for star IDs, see Table 2.8 below). For the analysis below, we have omitted seventeen observations with errors ≥ 1.0 km s^{-1} and three other observations which seem to be dubious.

The radial-velocity data are summarised in Table 2.8, as follows: columns 1-3, star idenfications: Küstner (1923), McNamara and Solomon (1981) and

Table 2.7: RVS Observational Log

Year	Nights	N_{obs}	Year	Nights	N_{obs}	Year	Nights	N_{obs}
1979	2	2	1986	3	21	1991	2	50
1981	2	4	1987	2	24	1992	1	15
1983	6	33	1988	2	40	1993	1	21
1984	16	160	1989	1	4	1995	9	33
1985	8	69	1990	2	31	1996	14	90
Total		71 nights				597 observations		

the present study; columns 4-5, V and V − I photometric data from the present CCD photometry; columns 6-11, the weighted mean velocity, the standard deviation of the mean, number of days between first and last observations, the number of observations used in the statistical analysis, the ratio E/I of the external over internal (expected) errors and the probability $P(\chi^2)$ (see below); columns 12-14, the membership probability by proper motion (McNamara and Solomon, 1981) and by radial velocity (Scott et al., 1995), and our own membership assessment from this study. A detailed discussion of the membership assessment appears in the next chapter.

Table 2.8: Radial Velocity Results

Identification[1]			Radial Vel.						Membership		
K	M	G	V_r	ε^2	No.[3]	D^4	E/I	$P(\chi^2)$	$P(\mu)$[5]	RV[6]	Rem.[7]
47		248								y	
57	306	1334	−54.00	72	1				84		M
72	315	15	−54.08	21	7	4300.85	1.37	0.125	96		MC
80		321	−53.61	24	7	4726.09	2.57	0.000			MV
136		336								y	
152	372	69	−54.98	36	3	186.14	0.49	0.924	97	y	MC
160		249	−59.54	20	8	4726.08	3.94	0.000		y	MV
193		149	−61.48	28	5	4240.16	0.97	0.579		y	U
200		271	−55.52	28	3	677.27	1.25	0.373			MC
202		273								y	
212	405	303	−54.81	36	3	305.19	0.64	0.843	85		MC
232		243	−54.36	33	4	3279.13	0.61	0.893		y	MC
244	431	264	−53.29	34	4	2492.20	1.27	0.304	97		MC
248			−54.35	39	1						
254	437	296	−56.50	34	4	2569.07	0.32	0.990	90		MC
255	441	185	−54.37	25	7	2582.03	1.54	0.047	98		MC
297		164	−57.17	23	9	4302.88	8.30	0.000		y	MV
301	475	97	−54.03	23	8	4368.95	1.99	0.001	97	y	MV
304	472	10	−12.98	35	3	48.79	0.30	0.980	0		NM
310			−52.74	71	1						
312	480	62	−12.93	35	4	4266.20	2.00	0.017	0	n	NM
319	485	181	−57.52	32	6	3308.94	17.84	0.000	98		MV
321	481	228	−53.83	39	3	1454.03	0.32	0.978	98	y	MC
327	494	138	−55.99	28	7	4308.98	1.69	0.016	98		MC
329	491	107	−54.35	23	7	4372.09	1.12	0.379	98	y	MC
337	504	108	−35.92	21	7	4674.83	1.39	0.116	0	y	NM
338	499	70	−54.84	15	16	4665.01	5.99	0.000	97	y	MV
347	506	221	−55.76	25	5	1838.02	1.95	0.010	96	y	MC

Table 2.8: *Continued*

Identification[1]			Radial Vel.						Membership		
K	M	G	V_r	ε^2	No.[3]	D[4]	E/I	$P(\chi^2)$	$P(\mu)$[5]	RV[6]	Rem.[7]
348	512	220	−53.36	27	5	2839.04	1.70	0.042	94	y	MC
353	509	131	−55.02	23	6	4743.18	1.57	0.054	97		MC
415	550	14	−52.98	17	10	4660.21	2.11	0.000	98		MV
416	552	266	−53.65	26	5	2926.18	1.13	0.408	98		MC
444	571	208	−53.39	28	5	2523.95	1.47	0.124	98		MC
450	573	110							0	y	
461	583	33	−53.92	16	14	6124.92	2.02	0.000	97	y	MV
466	588	82	−48.10	22	7	4737.76	1.44	0.089	3		NM
468	589	30	−55.82	15	12	4683.29	1.39	0.046	97	y	MC
476	592	300	−55.04	40	4	2140.17	0.86	0.699	89		MC
486	597	428							86	y	
489	598	36	−58.11	15	16	4298.92	13.42	0.000	84	y	MV
491	595	197	−58.11	32	5	4352.05	8.15	0.000	98		MV
494	604	18	−54.40	10	35	6232.78	1.74	0.000	94		MV
501	614	31	−54.74	15	14	5396.20	1.10	0.329	97	y	MC
526		212	−52.49	41	3	1454.00	0.76	0.765		y	MC
549	654	85	−53.70	26	6	4352.02	1.36	0.163	84	y	MC
555	662	241	−55.41	28	4	1099.16	1.33	0.261	98		MC
575	671	80	−55.29	20	5	5464.02	1.44	0.143	98	y	MC
593		225	−56.33	36	4	741.10	1.09	0.471		y	MC
601	700	99	−50.92	39	1				95	y	M
605	699	170	−49.21	28	4	4758.82	1.41	0.204	98	y	U
626	715	214	−54.36	24	7	4338.96	1.87	0.004	93		MV
637	723	94	−53.88	24	8	4306.94	9.70	0.000	97	y	MV
658	730	261	−54.85	30	5	741.02	0.88	0.682	97		MC
661	727	183							98	y	
665	738	207	−56.26	39	3	2187.03	0.85	0.692	97	y	MC
669	732	46	−54.57	18	10	5409.00	0.69	0.934	98		MC

Table 2.8: *Continued*

Identification[1]			Radial Vel.						Membership		
K	M	G	V_r	ε^2	No.[3]	D[4]	E/I	$P(\chi^2)$	$P(\mu)$[5]	RV[6]	Rem.[7]
675		95	−54.22	25	7	4381.86	1.12	0.371		y	MC
676	745	189	−56.12	18	11	4737.80	1.62	0.006	98		MV
684	743	218	−56.00	38	3	740.95	1.02	0.558	96	y	MC
692	757	230	−57.55	34	3	426.84	0.58	0.881	97		MC
707	762	213	−54.10	32	4	448.89	0.48	0.952	98		MC
709	758	124	−60.97	32	4	4305.07	0.48	0.954	0		NM
711	771	142	−55.46	30	7	4393.71	1.08	0.427	98		MC
716	775	187	−54.78	27	4	2445.26	0.99	0.566	98	y	MC
724	781	297	−55.18	28	7	4241.05	5.85	0.000	97		MV
732	783	154	−53.48	24	5	807.04	1.63	0.059	98	y	MC
737	786	322	−53.20	31	3	440.84	6.11	0.000	98		MV
751	788	20	−55.93	14	19	4385.75	3.08	0.000	98		MV
752	791	254	−55.75	37	3	449.08	0.11	0.999	98	y	MC
758	803	17	−20.22	46	1				0		NM
765	804	48	−55.83	19	11	4395.18	1.57	0.010	97	y	MC
778	812	256	−54.20	34	5	2118.05	1.00	0.548	98		MC
814	826	211	−55.06	28	6	4282.95	2.69	0.000	98		MV
827	836	174	−56.32	23	7	4282.05	6.07	0.000	98		MV
829		106								n	
841	843	161							37	n	
849	847	257	−52.89	39	3	2549.10	20.38	0.000	98		MV
859	853	126	−65.73	37	2	2545.18	6.76	0.000	98		U
865	862	141	−58.73	25	7	4238.05	7.43	0.000	96	y	MV
866	864	180	−51.99	26	4	4664.99	6.89	0.000	97	y	MV
875	873	216	−55.45	33	3	807.04	1.12	0.476	98		MC
897	881	188	−51.71	21	8	4731.90	2.35	0.000	97		MV
902	885	258	−54.51	51	2	48.80	1.29	0.434	98		MC
908	892	226	−53.69	25	5	2932.13	6.78	0.000	98		MV
950	927	182	−55.32	48	2	2492.24	1.58	0.286	95	y	MC

Table 2.8: *Continued*

Identification[1]			Radial Vel.						Membership		
K	M	G	V_r	ε^2	No.[3]	D^4	E/I	$P(\chi^2)$	$P(\mu)$[5]	RV[6]	Rem.[7]
957	935	246	−55.65	43	3	1392.19	1.47	0.231	98		MC
970	933	78	−54.86	21	9	4353.89	0.96	0.597	98		MC
971	946	28	−54.48	20	9	4662.05	1.22	0.215	98		MC
977	949	21	−52.00	21	8	4261.96	1.98	0.001	0		MV
978	944	125	−54.08	41	1				75	y	M
991	948	42	−12.05	48	2	4326.24	0.16	0.987	0	n	NM
1005	960	195	−54.72	39	3	4322.21	1.74	0.109	97	y	MC
1010	967	81	−54.74	46	1				98	y	M
1064	987	57							0	n	
1066	990	79	−55.02	22	8	4351.63	1.36	0.114	98	y	MC
1071	997	129	−56.10	28	5	4398.98	1.01	0.542	98	y	MC
1082	1001	186	−56.71	44	1				98		M
1091	1009	234	−54.37	39	3	334.00	0.70	0.809	95	y	MC
1092	1010	100	−66.04	51	2	1406.14	0.69	0.787	0	y	NM
1101	1013	198	−54.46	28	4	2546.03	0.72	0.816	98		MC
1107	1020	171	−56.55	28	5	2582.11	0.91	0.649	98	y	MC
1114		302	−52.66	34	2		1.90	0.164			MC
1147	1036	49	−54.98	40	2	88.81	1.40	0.375	98	y	MC
1149	1047	91	−40.61	32	4	4240.89	6.63	0.000	41		NM
1150	1044	179	−54.84	66	1				98		M
1196	1074	72	−54.99	28	5	1106.03	1.08	0.463	98	y	MC
1205	1086	59	−23.32	57	1				0	n	NM
1218	1092	50	−6.72	68	1				0	n	NM
1225	1098	146	−42.65	59	1				0		NM
1244	1118	163	−40.41	93	1				2		NM
1312	1158	165	−55.18	43	1				98		M
	108		−2.05	51	1						
	125	127	−24.23	67	1				98		U
	193	47	−56.34	37	1				98		M

Table 2.8: *Continued*

Identification[1]			Radial Vel.						Membership	
K	M	G	V_r	ε^2[2]	No.[3]	D[4]	E/I	$P(\chi^2)$	$P(\mu)$[5]	RV[6] Rem.[7]
	215	89	−57.37	51	1				90	M
	227	65	−52.91	48	1				70	M
	580	167	−55.07	48	1				97	M
	748	27	−66.50	36	1				98	M
	848	44	−35.39	35	1				21	NM
	866	66	−28.38	74	1				0	NM
	959	55	−38.57	48	2	35.73	1.17	0.504	0	NM
	994	45	−9.95	51	1				0	NM
	1121	12	−55.54	34	4	97.84	0.25	0.996	96	MC
	1244	369	−55.18	46	1				2	U

[1] Identification: K : Küstner (1923)
M : McNamara and Solomon (1981)
G : The present study

[2] Internal Error($\times 10^{-2}$ km s^{-1})

[3] The number of observations used in the statistical analysis

[4] Number of days between first and last observations

[5] Probability of proper motion membership (McNamara and Solomon 1981)

[6] Membership by radial velocity (Scott et al. 1995)

[7] Membership adopted in this study MC (members with constant velocity)
MV (members with variable velocity)
M (members with one or no velocity data)
NM (non-members)
U (stars with uncertain membership)

It is also worthwhile to note several points about the errors and the radial velocity statistics. The errors in Appendix A based on photon statistics will underestimate the standard deviation of the mean. Therefore the value of a typical RVS observational error for stars brighter than 9.0 magnitude where photon statistics are negligible, 0.4 km s^{-1}, is added in quadrature to each error in Appendix A before doing the statistical analysis. All weights are $1/error^2$. The $P(\chi^2)$ is the probability that the velocity variations are due to random observational errors. This is estimated by assuming that the errors have a Gaussian distribution and are purely statistical. A low $P(\chi^2)$ value suggests the star is affected by another source of velocity variation, and most probably it is spectroscopic binary. The radial velocities for 25 MV stars are plotted as a function of Julian Date in Fig. 2.7 and Fig. 2.8.

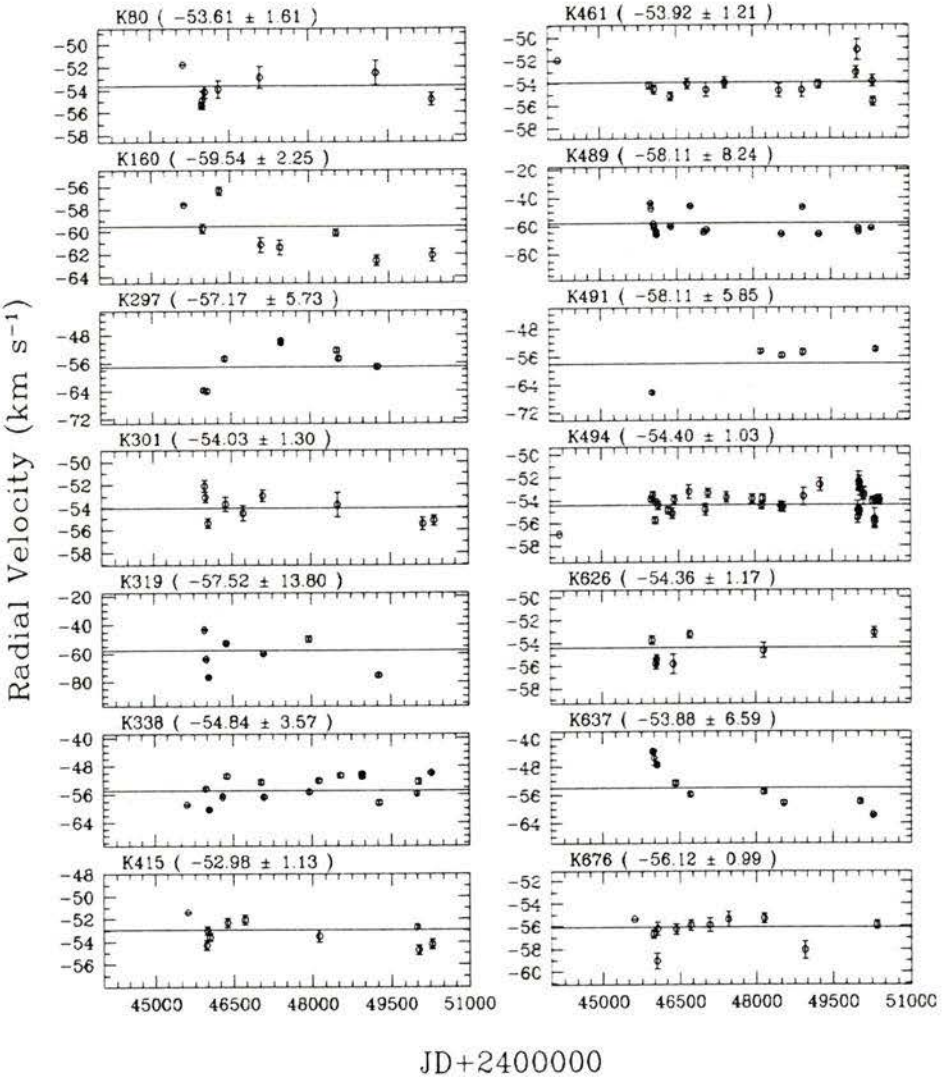

Figure 2.7: Radial velocities as a function of Julian Date for the proposed radial-velocity variables (MV) stars : Küstner number, Mean Velocity, and Standard deviation are shown at the left top of each panel. The horizontal line represents the mean of velocities measured over this interval.

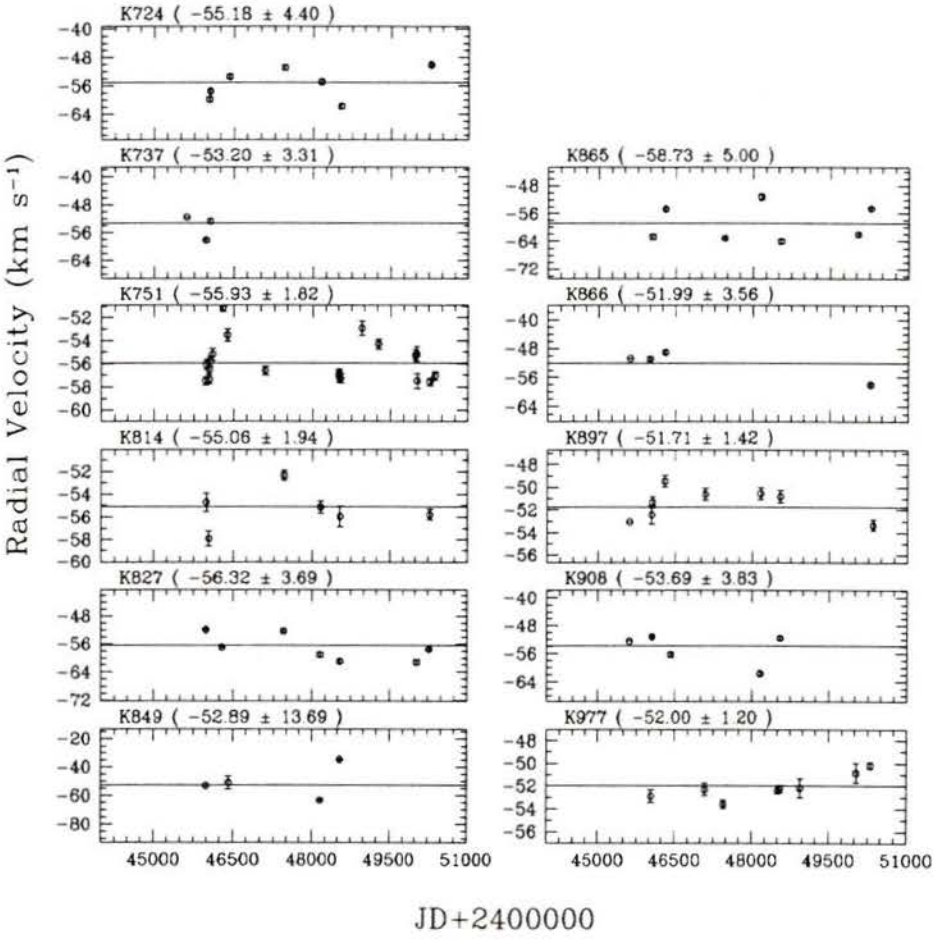

Figure 2.8: Same as Fig 2.7

Chapter 3

RESULTS and DISCUSSION

3.1 The CMD

Figure 3.1 shows the CMD for all 15617 stars with < 0.1 mag errors in the measured colors that were detected at least twice on both the V and I frames. Photometry was obtained for 5915 additional stars, but they are not used in the following analysis because of their relatively large errors ($\sigma(V-I) \geq 0.1$ mag) or because they had only one detection in either V or I. The stars rejected by one of these criteria are plotted in Figure 3.2, along with the cluster's main sequence fiducial fainter than $V = 14.0$. The latter is an eye-estimated, hand-drawn fit to the tight, well-defined lower main sequence population of NGC 7789 (see Fig. 3.1). Figure 3.3 shows the standard errors in V as function of V magnitude.

Our photometry covers a much larger area and extends to much fainter magnitudes than any previous survey. The CMD that we have obtained shows an extended giant branch, a well-defined "clump", numerous blue straggler candidates (see below), and a main sequence that extends down to at least $V = 21$. There is no evidence of any gap in the vicinity of

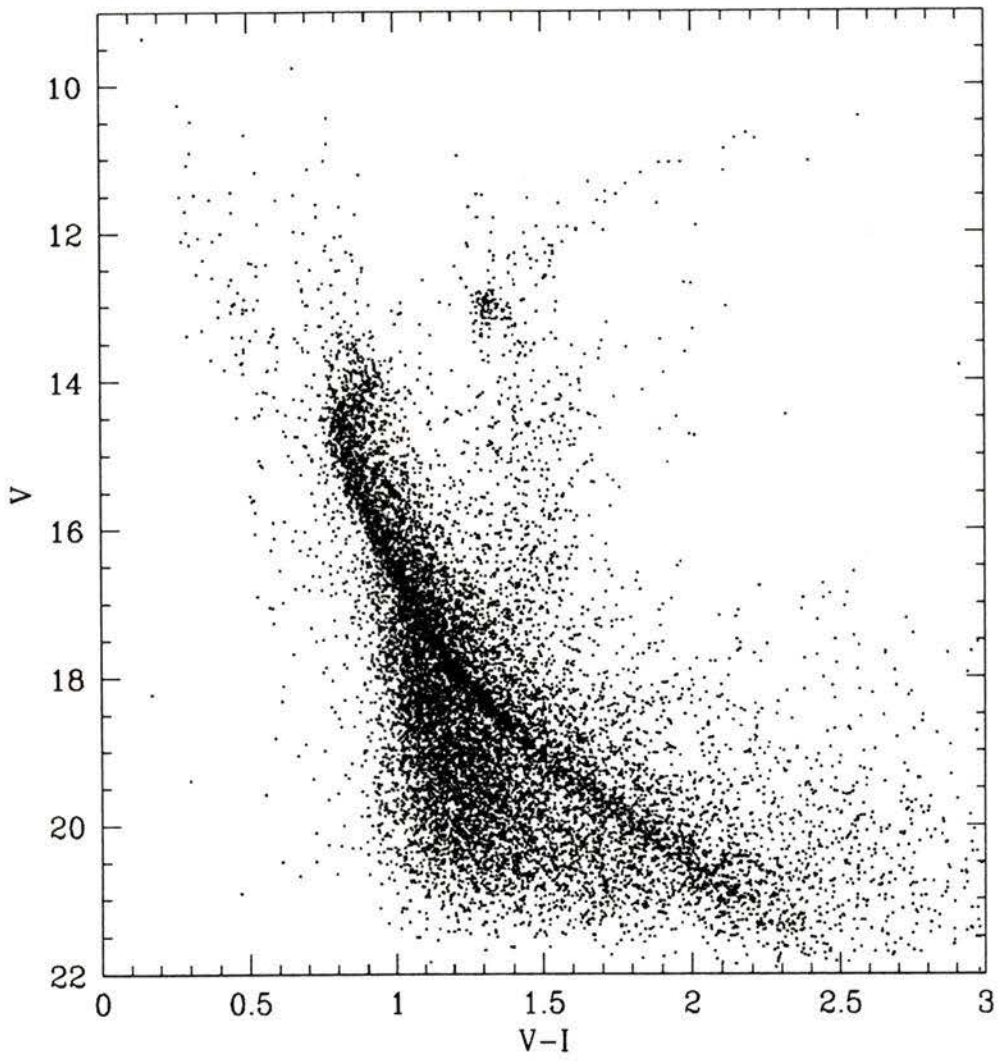

Figure 3.1: CMD for 15167 stars which were detected more than once in both V and I frames and also have $\sigma_{(V-I)} < 0.1$.

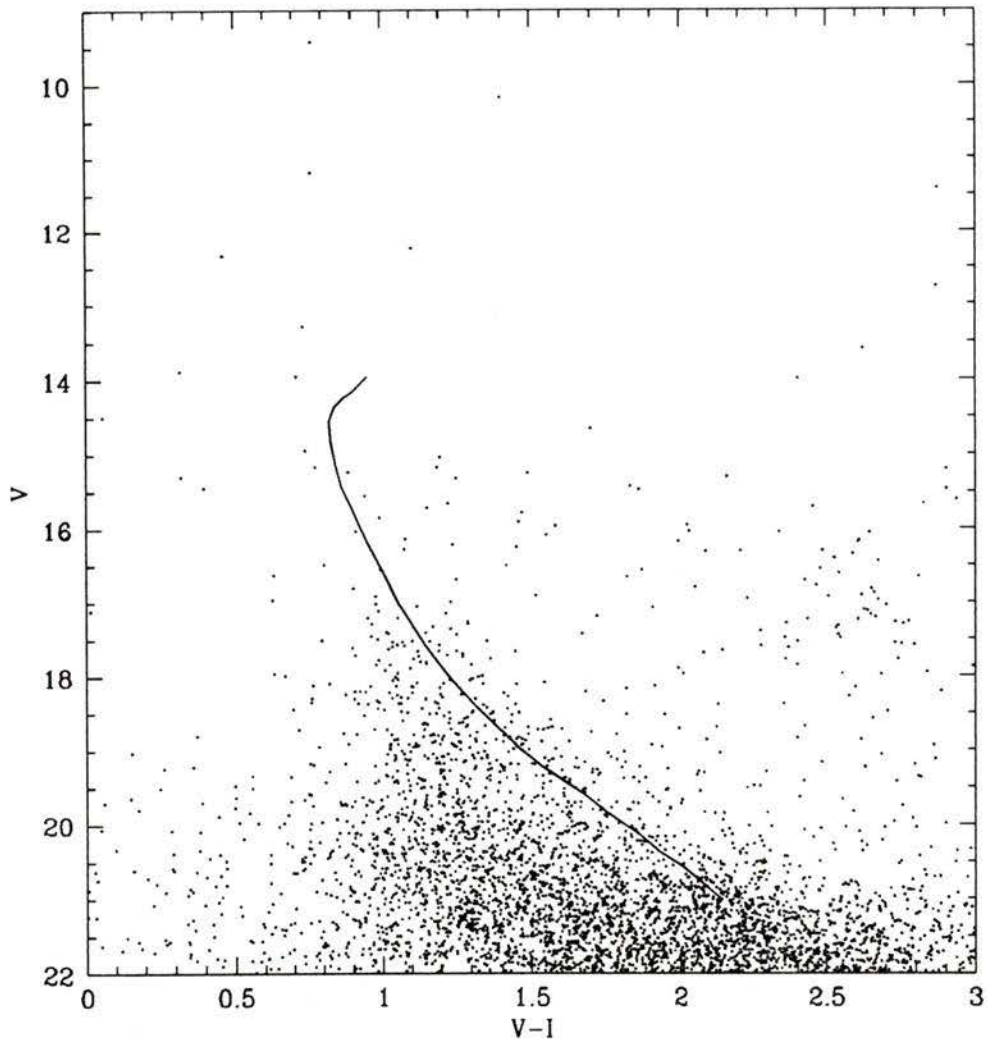

Figure 3.2: CMD for 5915 stars which are not used for the analysis because $\Delta(V-I) \geq 0.1$ or they were detected only once in either of the V or I frames. The solid line is the fiducial MS line which is obtained by eye fitting through the mean locus in Fig. 3.1.

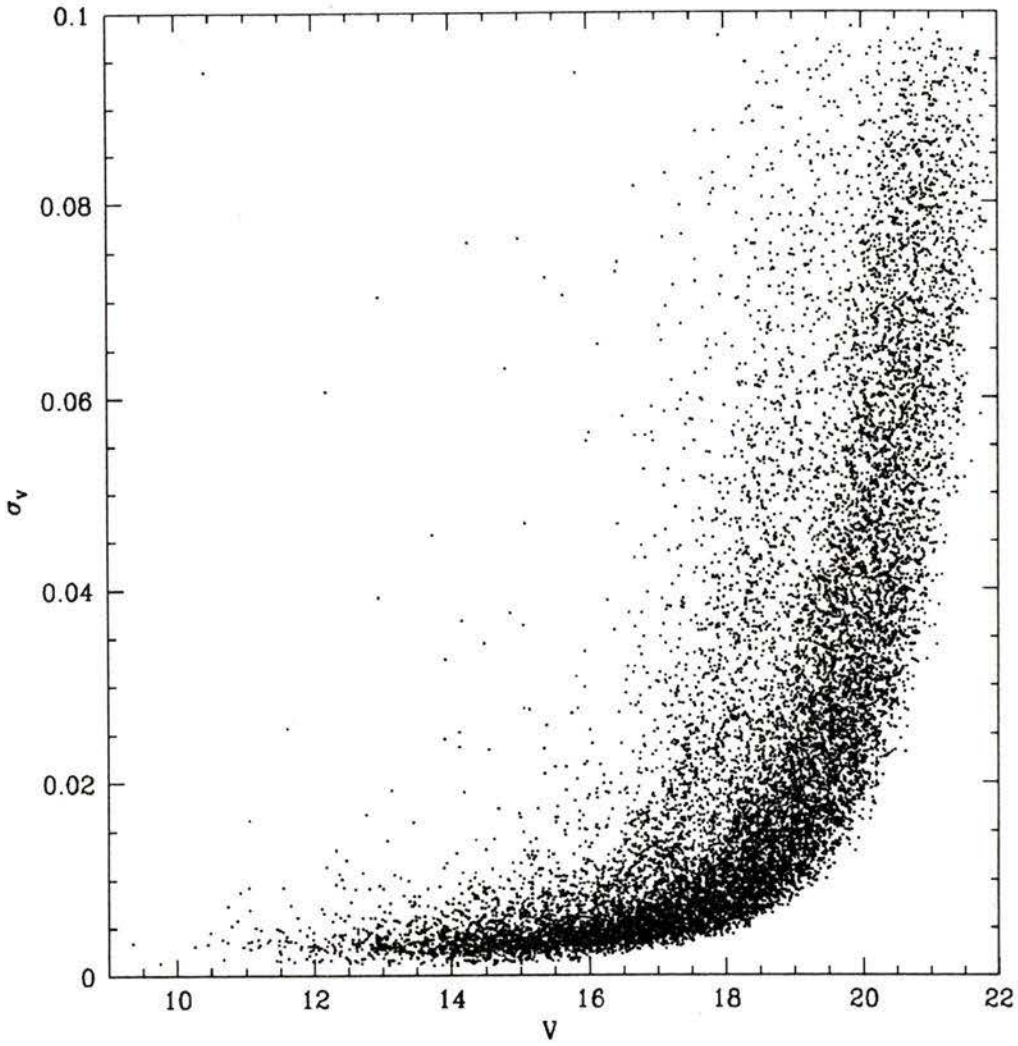

Figure 3.3: The standard errors in V plotted as a function of V magnitude.

the turnoff, though the upper end of the main sequence bends well to the red. This is reminiscent of the CMDs recently obtained for e.g., NGC 2420 (Anthony-Twarog et al., 1990) and NGC 752 (Daniel et al., 1994), and indicates substantial convective core overshooting in the main-sequence phase (see, e.g., Demarque et al. 1994). Field-star contamination, particularly in the color range $1.0 < V - I < 1.5$, is quite severe.

Figures 3.4 and 3.5 summarize what we know about the cluster membership. According to McNamara and Solomon (1981), those stars which are plotted as *plus signs* have a proper-motion membership probability $P(\mu) \geq 80\%$. Based on radial-velocity measurements made between 1979 and 1996, Gim et al. (1998) have identified 78 giant-star members: these are plotted as *open circles*, or denoted by the letter "V" to indicate that they are possible radial-velocity variables. Concerning the blue straggler candidates, the evidence seems to be quite strong that at least 16 of them (the *open squares* in Fig. 3.5) are members, according to our assessment (cf. Table 3.1) of the proper motion, radial velocity, photometric, and polarization work that has been done to date to determine the membership of 48 apparent blue stragglers in NGC 7789. As indicated in the final column of this table, the membership status of 13 of these stars was considered to be uncertain, so the actual number of *bone fide* blue stragglers could well be significantly greater than our estimate. Finally, it is worth noting that Jahn et al. (1995) found one pulsating blue straggler and 15 short-period variables as the result of observing NGC 7789 over four consecutive nights.

Table 3.1: Membership of blue stragglers in NGC7789

Identification[a]			PM[b]		RV[c]					PHOT[d]		$\mathcal{P}^e$	A[f]
K	M	G	P	Mc	SS	SH	D	MPR	ML	TT	MR	B	
2	257	396		98					no	no			U
68	317	498		76					no	m			U
88	325	348		98					no	m		m	U
144	361	425		0	no								N
168	377	560		77	no		no		fr	m		u	U
192	389	479		52					fr	m		u	U
197	396	381	38	46	m				no			u	N
234	419	421	78	0	m							no	N
246	432	16		0				no(c)			no	no	N
282	460	114	91	97		m	m	m(v)	fr	m	m	m	M
316	482	549	93	98			m		m			m	M
325	489	1126		98									U
342	502	166	91	96	m	m	m	m	fr	m		m	M
349	500	404	92	0	m							no	N
351	514	447	92	0								no	N
371	518	277	83	98	no	m	m	m(c)	m	m	m	m	M
409	543	295	82	53	m	m	no		no	m	m	u	N
430				0								no	N
453	574	204	92	98	m	m	m	no(c)	fr	m	m	m	M
462	577	298		0				no				no	N
635	712	282	92	8								no	N
677	747	43	92	53		m	no	no(c)	no	m?	m	m	N
696	752	558	86	98					fr	m		m	M
746	789	231	92	98			m		m	m		m	M
758	803	17		0								no	N
799	817	76		0	no			no(c)			no	no	N
889	879	61		0				no(c)			no	no	N
906	893	191		0								no	N
934	913	311		78					no	m		u	N
1047	981	140		96					fr		m	u	M
1095	1011	589	91	98					m			m	M
1119	1026	255	92	0								u	N
1168	1054	534	54	95	m		m		m	m?		m	M

Table 3.1: *Continued*

Identification[a]			PM[b]		RV[c]					PHOT[d]		$\mathcal{P}^e$	A[f]
K	M	G	P	Mc	SS	SH	D	MPR	ML	TT	MR	B	
1208	1090	74		0								no	N
1211	1088	73	91	97	m	m	no		no	m	m	m	U
1270	1133	384		98			m		m	m		m	M
1288	1142	314		92					fr	m			M
1309	1161	39		0								no	N
	99	104		86					no	no	m		U
	144			67					fr	m?			U
	172			89					no	no			U
	210			90					no	no			U
	238	168		94			no		no	no			U
	459	52		90			m		fr	m	m		M
	511	29		98			no		fr	m	m		M
	808	345		94			no		fr	m?			M
	1060	23		97			no		fr	m?			M
	1251	176		71			no			m			U

Notes — v: variables, c: constants, fr: fast rotators in the columns 9 and 10;
m: members, no: non-members, u and m?: stars with uncertain membership

[a]Identification: K : Küstner (1923)
M : McNamara and Solomon (1981), G : The present study
[b]Membership probability by proper motion:
P: Pendle (1975), Mc: Mcnamara (1980)
[c]Membership by radial velocity:
SS: Strom and Strom (1970), SH: Stryker and Hrivnak (1984)
D: Drilling and Schönberner (1987),
MPR: Manteiga et al. (1989), ML: Milone and Latham (1994)
[d]Photometry:
TT: Twarog and Tyson (1985), MR: Manteiga et al. (1991)
[e]P : Polarization: B: Breger (1982)
[f]Adopted membership: M (members), N (non-members),
U (stars with uncertain membership)

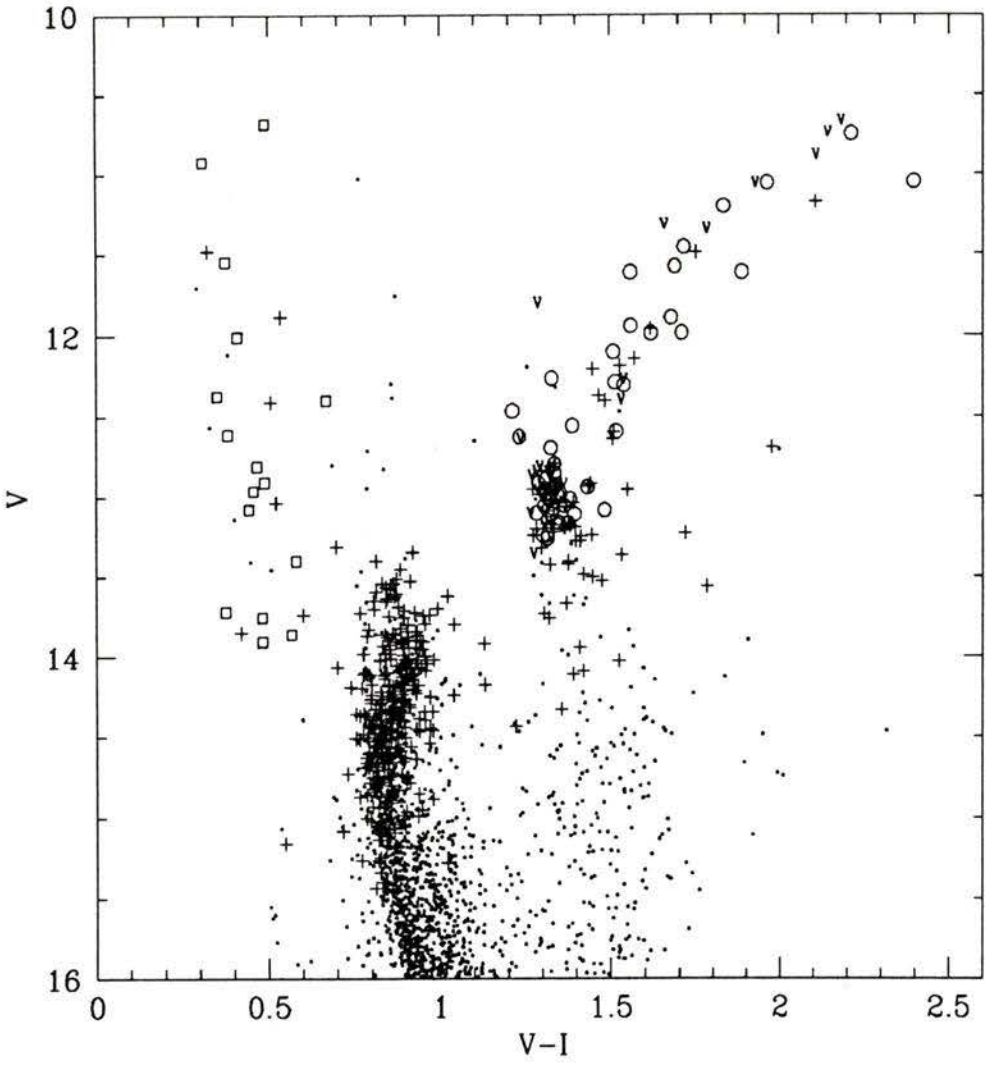

Figure 3.4: A CMD which incorporates membership information for giant branch, blue straggler and upper-main sequence stars, as follows: *plus signs*: proper motion members (McNamara and Solomon, 1981); *open circles* and *"V"*: radial velocity members including velocity variables (Gim et al., 1998); *open squares*: blue stragglers (see Table 3.1). *Dots* are stars for which no membership information other than their location in the CMD is available.

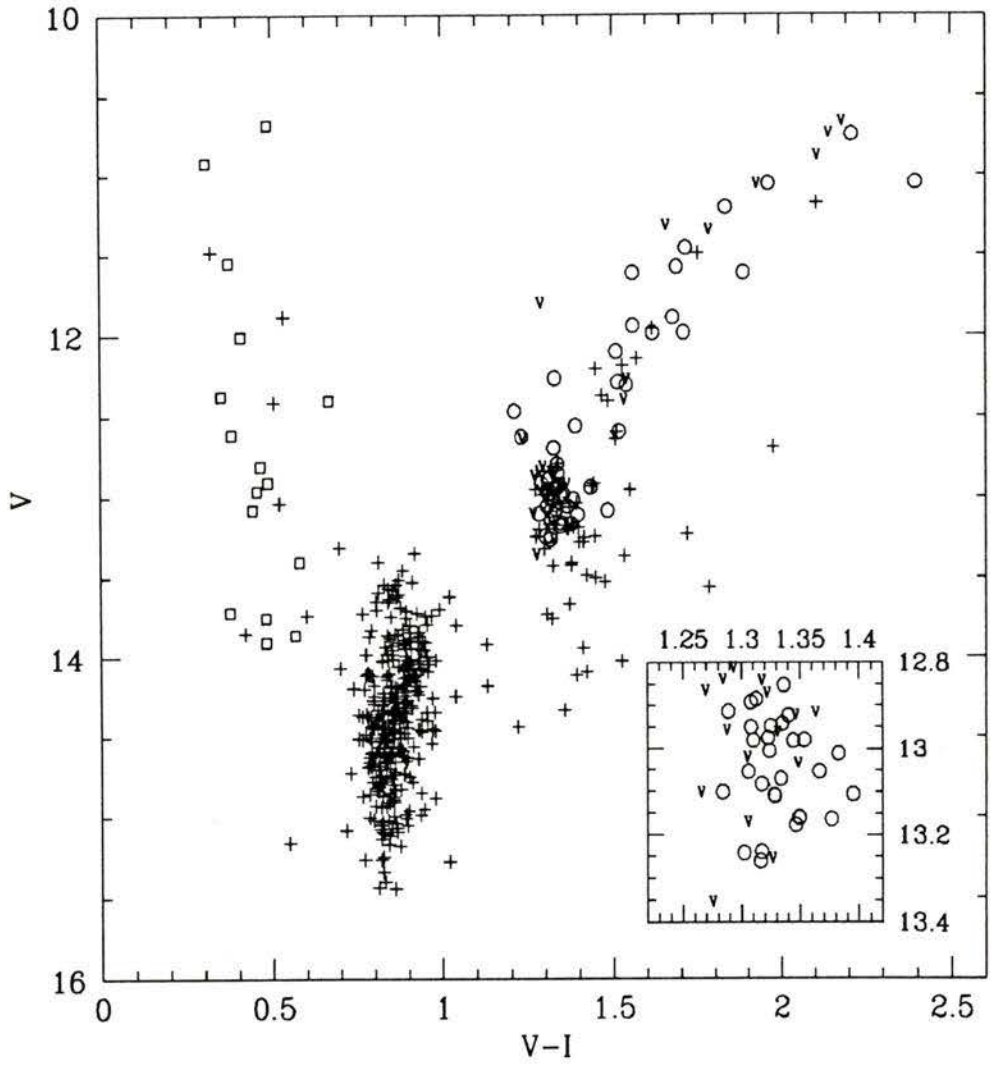

Figure 3.5: Same as Fig. 3.4, but for only those stars thought to be members. The clump star region is shown in the inset box with the expanded scale.

3.2 Analysis of the NGC 7789 CMD

3.2.1 Comparison with the M67 CMD

As indicated in Table 1.1, the available metallicity estimates for NGC 7789 range from [Fe/H] ≈ -0.3 to 0.0 (solar), whether determined spectroscopically or photometrically. As the uncertainty in this quantity is quite large, making it difficult to choose which models should be compared with the photometry, it is clearly desirable to try to constrain this parameter more tightly. One way to do this is to compare, in an age- and reddening-independent way, our CMD for NGC 7789 with that of another open cluster having a similar metallicity. M 67 is an obvious choice for such a comparison cluster because it has a well-defined CMD on the $(V, V-I)$–plane (Montgomery et al., 1993) and because its metal abundance is very well determined at [Fe/H] ≈ -0.05: most recent determinations (e.g., Nissen et al., 1987; Hobbs and Thorburn, 1991; Friel and Janes, 1993) are within ± 0.05 dex of this estimate.

To carry through the analysis, let us assume that the stars in NGC 7789 have exactly the same chemical composition as those in M 67. If that is the case, and if we superpose the cluster CMDs in such a way as to force the core He-burning "clump" stars in both clusters to have the same mean magnitude and color, which one might naively expect, then their respective lower main sequence populations should also overlay one another. As shown in Figure 3.6, such a coincidence is not obtained: the lower main sequence of NGC 7789 is redder than that of M 67 (at a fixed magnitude), which indicates that either our assumption of a common metallicity is incorrect, or the clump stars in NGC 7789 have not been properly fitted to those in M 67. The two

clusters have quite different ages and, according to the predictions of stellar models, the NGC 7789 clump should be somewhat bluer and brighter than M 67's, if the stars in both clusters undergo comparable amounts of mass loss prior to the core He-burning phase[1]. Our ZAHB for solar abundances (see below) indicates, for instance, that a $1.6\mathcal{M}_{\odot}$ model is 0.17 mag brighter and 0.04 mag bluer (in $V-I$), than one for $1.2\mathcal{M}_{\odot}$.

Suppose we adopt these offsets in positioning the NGC 7789 clump relative to that of M 67 and then intercompare the lower main sequence fiducials of the two clusters. The result is Figure 3.7, and once again we find that the unevolved stars in NGC 7789 are redder than those of M67 (at a fixed $V > 15$). [The slope of the theoretical ZAHB is predicted to be nearly the same as the slope of the lower main sequence; consequently, the change in V largely compensates for the change in $V-I$ (of the clump stars) and the relative main-sequence locations of the two clusters are not altered appreciably.] Thus, the clump stars in NGC 7789 *must* be significantly bluer and/or *fainter* than those in M 67. If the reverse were true, then the main sequence of NGC 7789 would be well separated from (and redder than) that of M 67, which would imply that the former has much greater than solar abundances of the chemical elements — something for which there is no observational support.

According to, e.g., Friel and Janes (1993) and Twarog et al. (1997), NGC 7789 is approximately 0.1 dex more metal-poor than M 67, which would suggest that NGC 7789 has [Fe/H] $\gtrsim -0.2$. However, the uncertainties

[1]As shown by e.g., Demarque and Hirshfeld (1975), the zero-age horizontal branch (ZAHB) for stars more massive than $\approx 1.0\mathcal{M}_{\odot}$, runs from the lower right to the upper left on the C-M plane (in the direction of increasing mass).

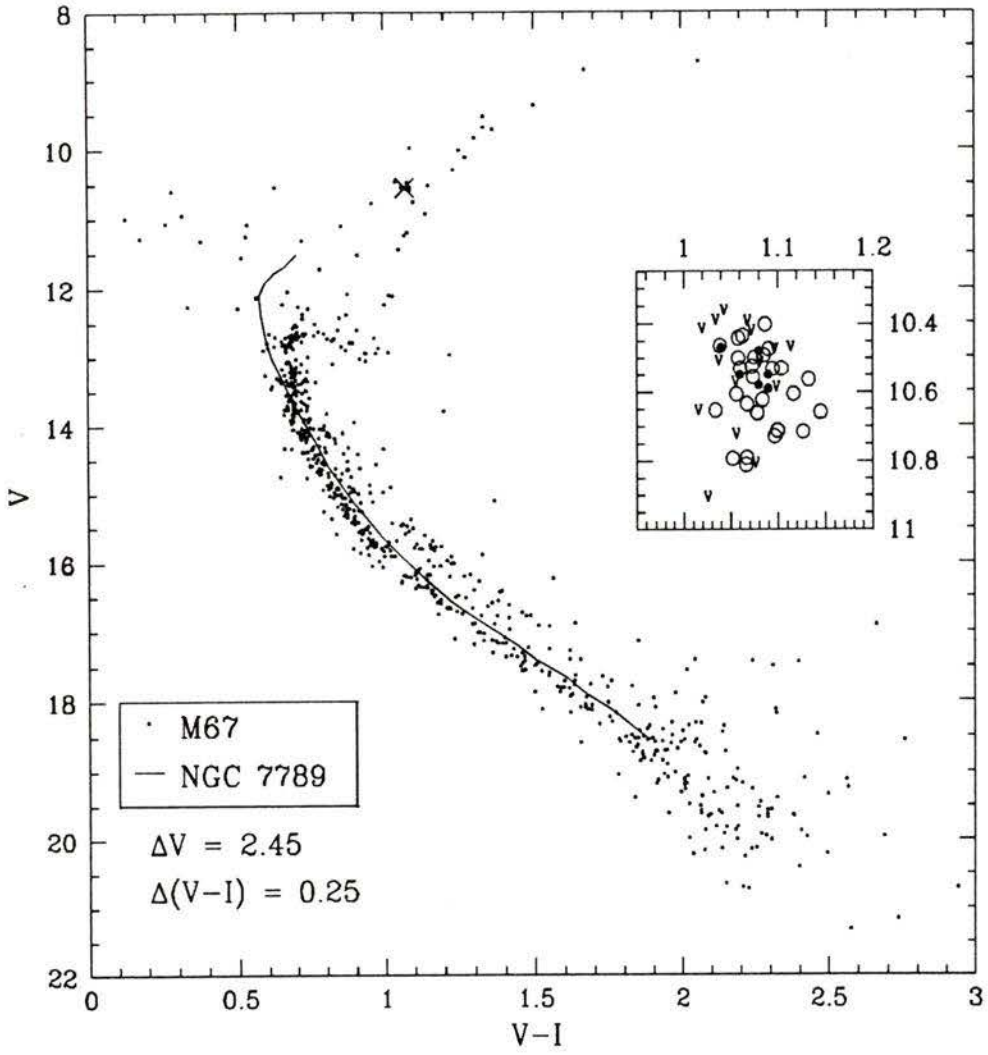

Figure 3.6: CMD of M 67 (Montgomery et al., 1993) overplotted by the fiducial sequence for the NGC 7789 MS and its clump (*large cross*), which are shifted by $\Delta(V-I) = 0.25$ and $\Delta V = 2.45$ to match M 67. As shown in the inset box, these adjustments produce an approximate centering centering of the NGC 7789 clump onto that for M 67. The small *filled circles* represent the observed clump stars in M 67 while all other symbols represent NGC 7789 clump stars.

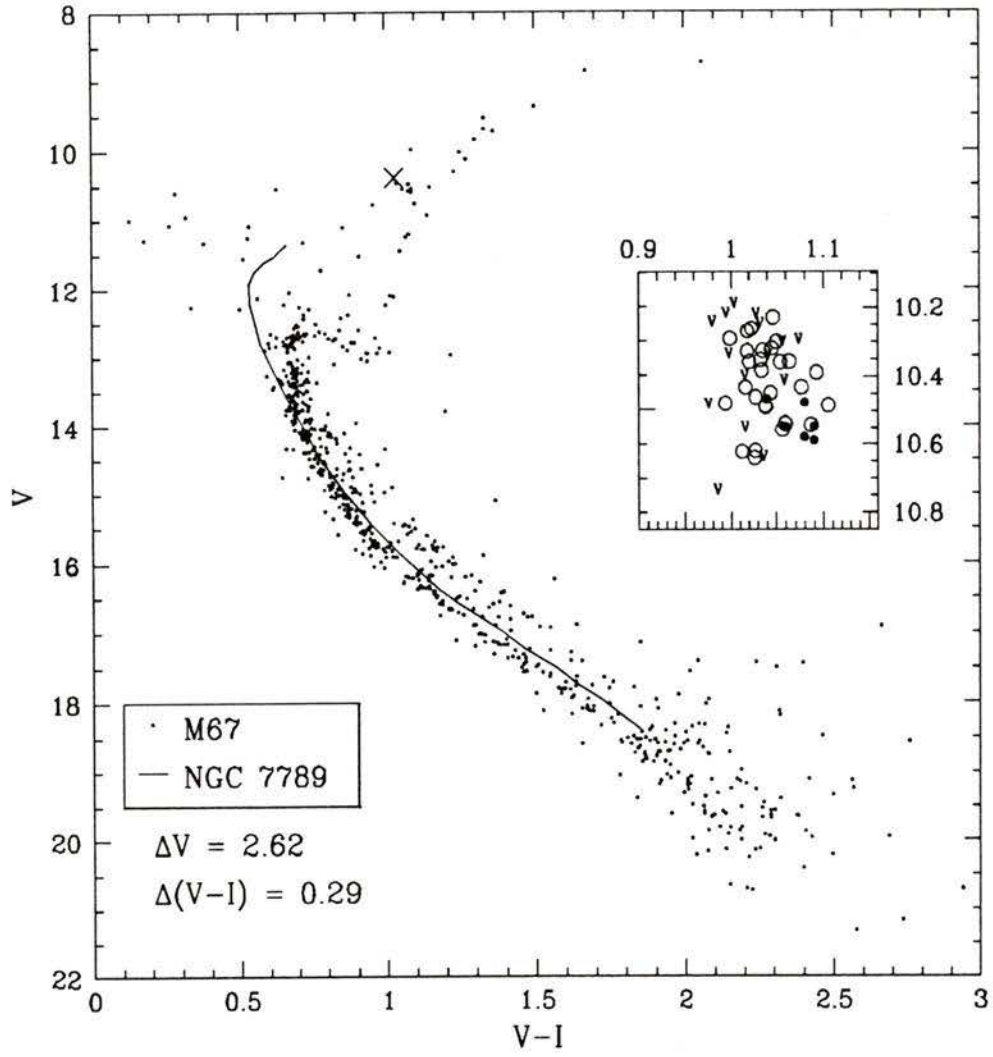

Figure 3.7: As Fig. 3.6, but NGC 7789's data are shifted by $\Delta(V-I) = 0.29$ and $\Delta V = 2.62$. As shown in the inset box, these offsets cause the M 67 clump stars to be redder and fainter, in the mean, than their counterparts in NGC 7789. This approximately consistent with the expectations from theoretical ZAHB models between 1.2 and $1.6\mathcal{M}_{\odot}$ (which assumes some mass loss).

are such that both clusters could have [Fe/H] $\approx$ 0.0, and since it useful to explore how the interpretation of a given CMD depends on the assumed metallicity, models for both [Fe/H] = 0.0 and -0.2 will be compared with the observations.

3.2.2 Stellar Model Fits

For their study of NGC 6819, Rosvick and VandenBerg (1998) computed several sets of models for solar abundances: reference should be made to that study for a description of the evolutionary code that was used. Worth emphasizing is the fact that those models were carefully normalized to the Sun and that convective overshooting has been treated using a parameterized version of the Roxburgh (1989) criterion. To be specific, we have determined the radius of a convective core, r_{cc}, from the requirement that

$$\int_0^{r_1} \mathcal{F}_{\rm over}(L_{\rm rad} - L)\frac{1}{T^2}\frac{dT}{dr}dr + \int_{r_1}^{r_{cc}} (2 - \mathcal{F}_{\rm over})(L_{\rm rad} - L)\frac{1}{T^2}\frac{dT}{dr}dr = 0 \ ,$$

where $\mathcal{F}_{\rm over}$ is a parameter with allowed values in the range $0.0 < \mathcal{F}_{\rm over} \leq 1.0$, L is the total luminosity produced by nuclear reactions, $L_{\rm rad}$ is the radiative luminosity, and the other symbols have their usual meanings.[2] The

[2]In its most general form, Roxburgh's (1989) criterion contains two integrals with limits from $r = 0$ to $r = r_{cc}$ — one which is equivalent to the above with $\mathcal{F}_{\rm over} = 1.0$, and the other which properly accounts for energy dissipation. Where the difference between these two integrals vanishes is the correct radiative-convective boundary. However, the second integral requires the solution of the full set of turbulent equations that applies to a convective core and, consequently, it is not easily evaluated (though see Canuto and Christensen-Dalsgaard 1998). The parameterized criterion that we have solved is, in contrast, extremely easy to evaluate and, although the "trial and error" approach must be used to determine which value of $\mathcal{F}_{\rm over}$ produces the most realistic models to fit to an observed CMD, the computational effort is still rather small. Although our *ad hoc* way of limiting the extent of convective overshooting does not add very much to the physics of convection, an evaluation of $\mathcal{F}_{\rm over}$ does provide some empirical information on the relative importance of the dissipation term.

radius r_1 is the classical radiative-convective boundary; i.e., the point where $\nabla_{\rm ad} = \nabla_{\rm rad}$ (and $L = L_{\rm rad}$). Because $L < L_{\rm rad}$ in the overshooting region ($r_1 < r \leq r_{cc}$) *and* because the dissipation is always positive, consistency demands that the factor $\mathcal{F}_{\rm over}$ in the first integral be replaced by the factor $(2 - \mathcal{F}_{\rm over})$ in the second integral. Setting $\mathcal{F}_{\rm over} = 1.0$ clearly recovers the integral equation that applies when viscous dissipation is neglected altogether (see Roxburgh's paper): this case corresponds to the maximum possible amount of overshooting. The minimum size of a convective core is obtained when the radiative-convective boundary is determined from the Schwarzschild criterion. (In what follows, the non-overshooting calculations are labelled "$\mathcal{F}_{\rm over} = 0.0$" even though, in this special case, the overshooting subroutine is bypassed.)

One goal of this investigation is to determine which value of $\mathcal{F}_{\rm over}$ leads to the best agreement between theoretical models and the observed CMD of NGC 7789. Knowing this will provide a valuable calibration point for the variation of this parameter with mass (and possibly [Fe/H]), which we hope to derive from similar considerations of other open clusters that encompass a wide range in age and metal abundance. But the distance scale is an important ingredient in such analyses. In a highly-reddened cluster like NGC 7789, it is arguably the best approach to infer the distance modulus from the magnitude of the clump stars. Based on published observations for many open clusters, Twarog et al. (1997) have suggested that "over the age range from NGC 7789 to Mel 66 (approximately 1 to 5 Gyr), the mean M_V is 0.6 ± 0.1". Since the mean magnitude of the clump in NGC 7789 is $V = 13.0 \pm 0.05$ mag (see Fig. 3.5), the Twarog et al. M_V estimate implies that

the apparent distance modulus of NGC 7789 is close to 12.40 mag. The reddening then follows from the requirement that the predicted zero-age main sequence, which is independent of whether or not overshooting occurs, match the observed main sequence for the unevolved stars, i.e., those fainter than $M_V \sim 4$. (Deriving this quantity from a main-sequence fit to stellar models should be especially reliable because the theoretical calculations have been normalized to the Sun: we assume $M_{V,\odot} = 4.84$, $(B-V)_\odot = 0.64$, and $(V-I)_\odot = 0.72$).

Figures 3.8 and 3.9 illustrate fits of evolutionary tracks for $\mathcal{F}_{\rm over} = 0.0$ and 1.0, respectively, to the NGC 7789 CMD assuming $(m-M)_V = 12.40$ and $E(V-I) = 0.38$. The tracks are the same as as those used by Rosvick and VandenBerg (1998) in their analysis of NGC 6819 BV photometry, though we have extended those grids to include evolutionary sequences for 1.8 and 1.9 $\mathcal{M}_\odot$ stars. It is immediately apparent that neither set of models correctly predicts the observed TAMS ("terminal age main sequence"). The predicted TAMS, which is indicated by the nearly vertical *solid* curve connecting the red end of the hook feature, is either much too blue, in the case of the non-overshooting models, or somewhat too red, in the case of the models for $\mathcal{F}_{\rm over} = 1.0$: this is in comparison with the observed location of the bright end of the cluster main sequence. An intermediate amount of overshooting is clearly indicated and, as shown in Figure 3.10, models that assume $\mathcal{F}_{\rm over} = 0.5$ provide quite a good match to the observed TAMS.

The tracks for masses from 1.1 to 1.9$\mathcal{M}_\odot$ were extended to include the giant-branch phase and, using a modified version of the Bergbusch and VandenBerg (1992) interpolation code (see Bergbusch and VandenBerg, 1998),

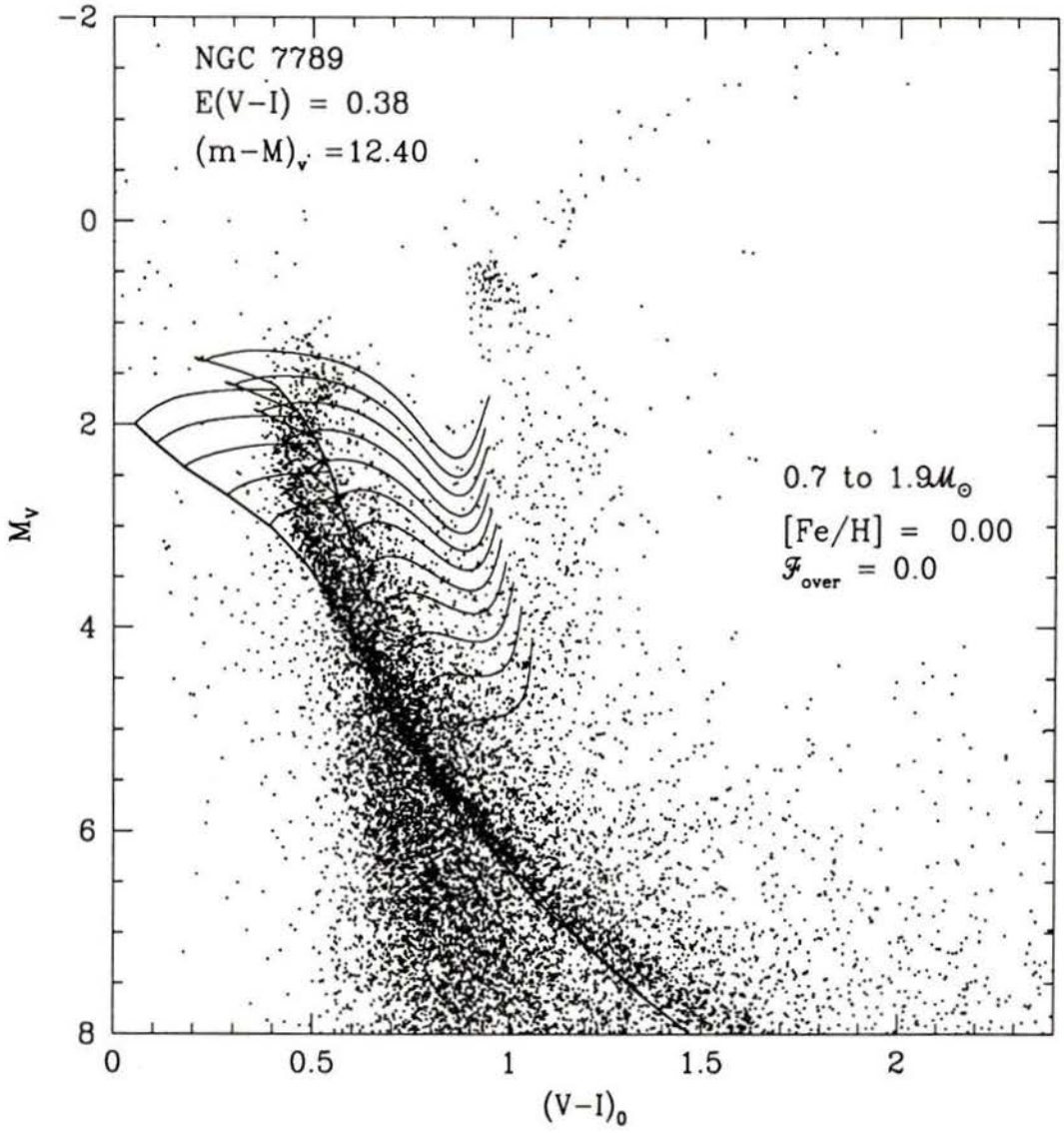

Figure 3.8: An NGC 7789 CMD on which the evolutionary tracks for $0.7 - 1.9\mathcal{M}_{\odot}$ are superimposed. The adopted reddening and distance modulus are as noted. ZAMS and TAMS points are connected by a thick solid curves. The line connecting the TAMS points does not fit the observations, which suggests that stellar models without overshooting are not appropriate.

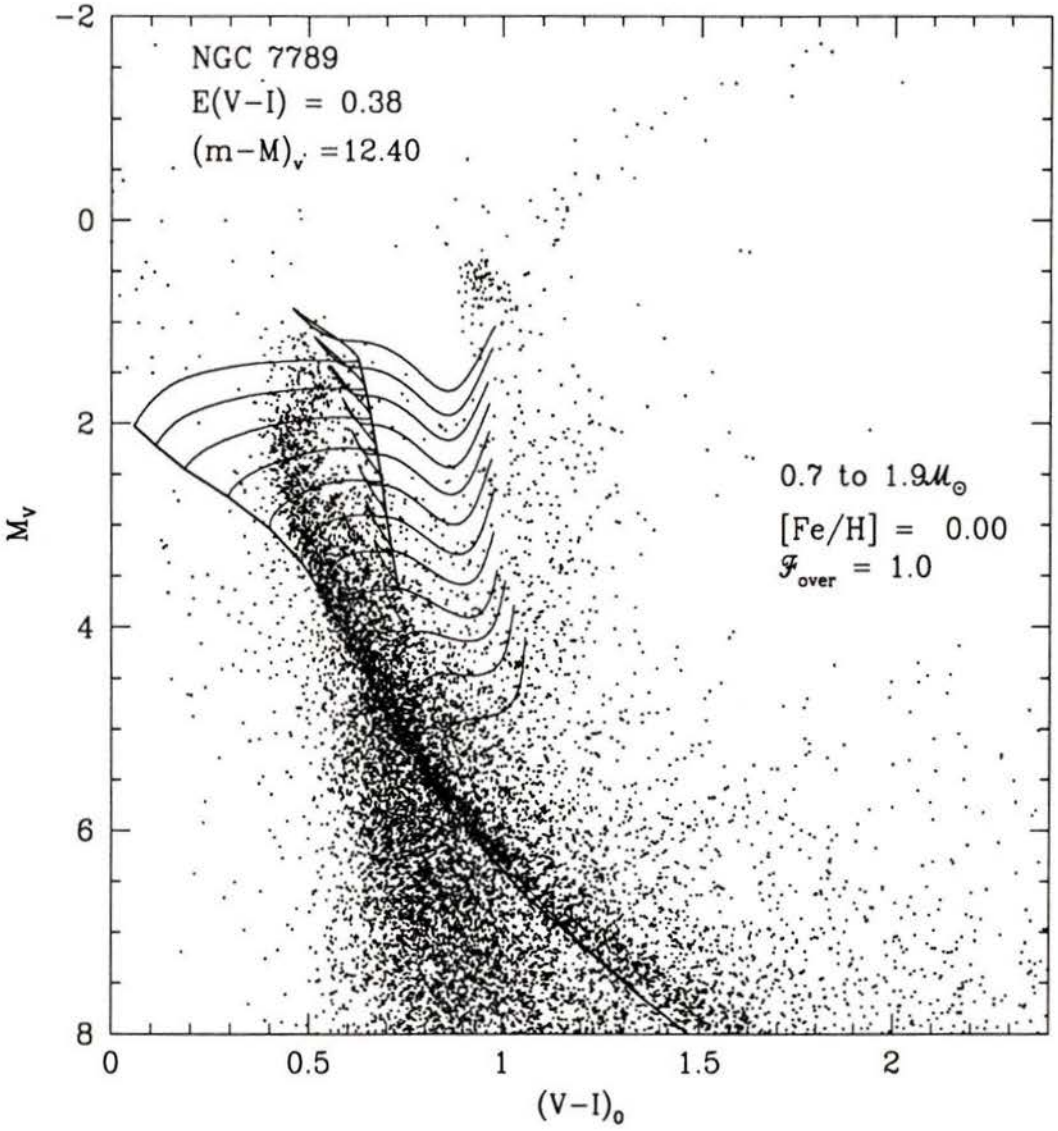

Figure 3.9: As Fig. 3.8, but for models with the maximum possible extent of overshooting according to the Roxburgh (1978, 1989) criterion. The predicted TAMS clearly fails to match the observed one, indicating that too much convective overshooting has been assumed.

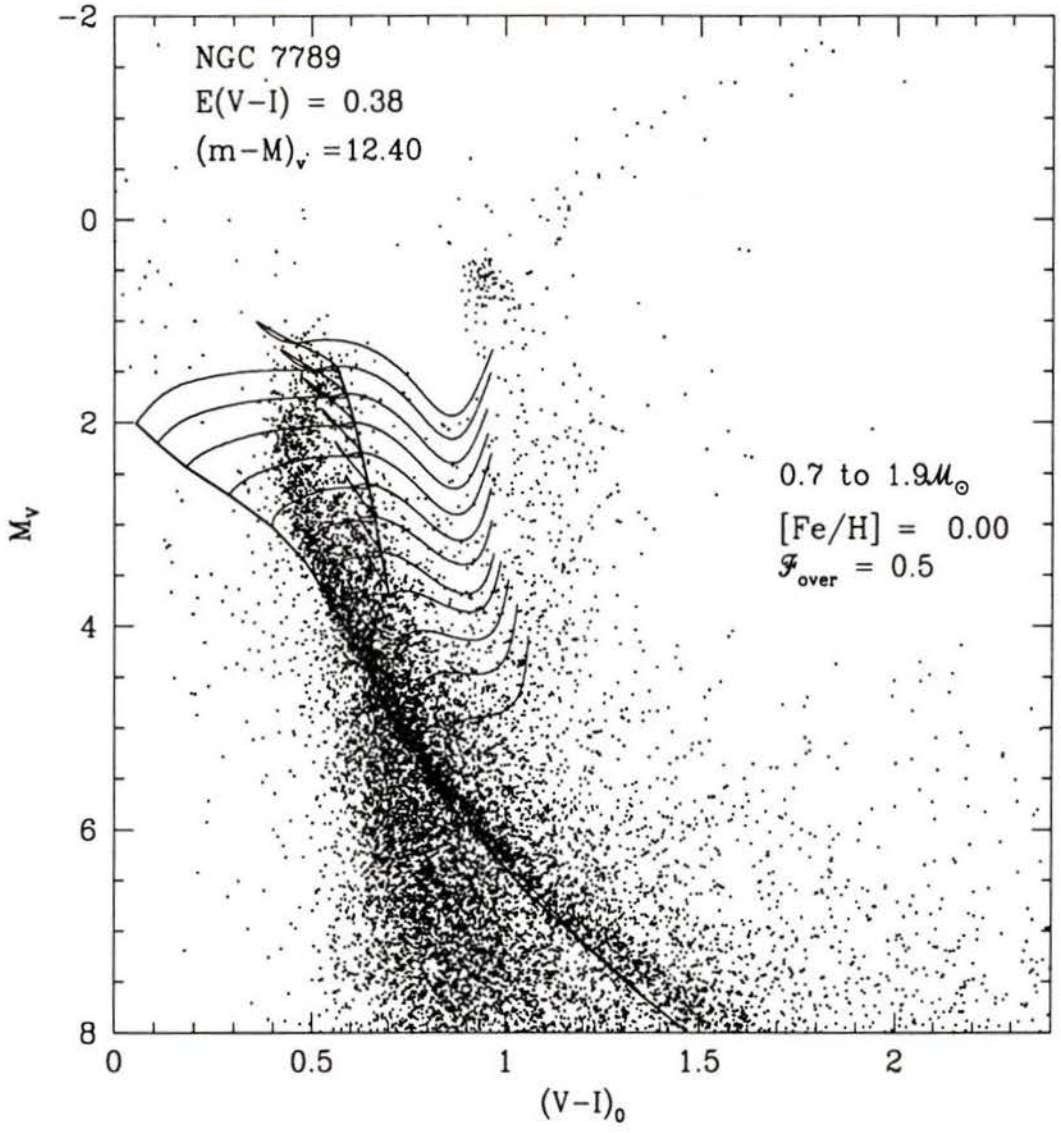

Figure 3.10: As Fig. 3.8, but for models with an intermediate amount of overshooting according to the Roxburgh (1978, 1989) criterion. The predicted TAMS now reproduces the observed one well.

isochrones were produced for a suitable range in age. A 1.5 Gyr isochrone is superposed on the photometry in Figure 3.11, on the assumption of the same distance modulus and reddening that were adopted in the previous three figures. This is clearly not a "best-fit" isochrone as it is readily apparent that one for a slightly younger age is needed to fit the turnoff observations. However, besides being too red, the predicted giant branch at an age of 1.5 Gyr is not quite as extended as it needs to be to match the observed RGB, and that for any younger age will be even stubbier. It is one of the well-known consequences of convective overshooting on the main sequence (see Bertelli et al., 1986, and references therein) that the transition mass between quiescent and violent helium ignition (the so-called "helium flash") is reduced in comparison with the predictions of canonical, non-overshooting models. The approach to this transition mass from the low mass side is signalled by a fairly abrupt and rapid decrease in the length of the RGB (see, e.g., Sweigart et al., 1989). Thus, whether or not an intermediate-age cluster shows an extended giant branch provides a useful constraint on its distance and age (or on the importance of convective overshooting), as was first pointed out by Barbaro and Pigatto (1984). In order for our overshooting models to match both the turnoff morphology and the well-developed giant branch possessed by NGC 7789, we are forced to conclude that the cluster distance modulus must be less than $(m - M)_V = 12.40$.

A more favorable comparison between the solar-abundance models and the NGC 7789 CMD is obtained if $(m - M)_V = 12.20$. This is illustrated in Figure 3.12, which indicates that a value of $\mathcal{F}_{\rm over} = 0.5$ still provides a good fit to the observed TAMS, and in Figure 3.13, which shows that a 1.6

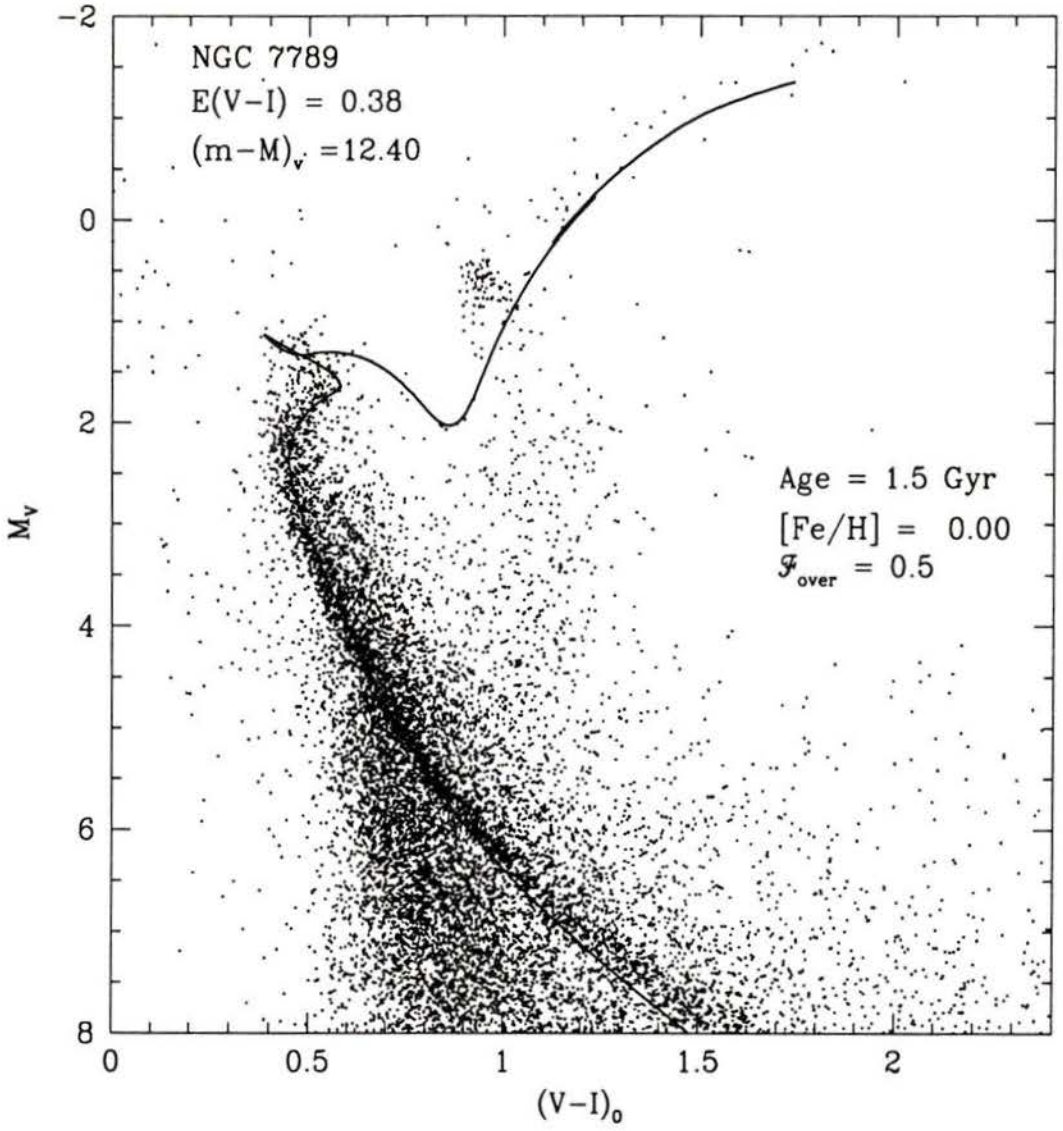

Figure 3.11: The CMD for NGC 7789 with an isochrone for 1.5 Gyr superimposed. While the match between theory and observations is generally good, the theoretical giant branch does not extend far enough to fit the observed red-giant branch.

Gyr isochrone faithfully reproduces the cluster's main sequence and RGB fiducials. However, the comparison between theory and observations is still not completely free of difficulty. For the first time in this analysis, we have superposed a theoretical ZAHB locus on the photometry and its location relative to that of the core He-burning stars seems problematic. This ZAHB consists of a sequence of 29 models having the same helium core mass, $\mathcal{M}_c$, but a range in total mass from $0.50\mathcal{M}_\odot$, at the blue end, to $1.8\mathcal{M}_\odot$, at the bright end past the red "nose". If no mass is lost in the precursor evolutionary phases, the clump stars should populate the bright end of the ZAHB: mass-losing stars should be fainter and redder than this point, eventually becoming bluer again if the mass loss has been severe. But there are many stars lying along the extension of the ZAHB to bluer colors and brighter magnitudes.

The same "anomaly" was found by Rosvick and VandenBerg (1998) in the case of the $\sim$ 2.4 Gyr open cluster NGC 6819. They suggested that the brightest of the clump stars might be the descendants of blue stragglers, given that there is a confirmed blue straggler population in that cluster. NGC 7789 also contains significant numbers of such stars (see Figs. 3.4 and 3.5) and one cannot help but speculate that their progeny might lie along the extension of the ZAHB to higher mass (if blue stragglers are significantly more massive than the cluster turnoff stars). However, there appears to be too many excessively bright clump stars for this to be the entire explanation.

We may, of course, be placing too much reliance on the accuracy of the ZAHB models. The reader will notice that the flat part of the ZAHB is very faint. This is for the reason that the predicted core mass in the overshooting models, particularly when the total stellar mass approaches the

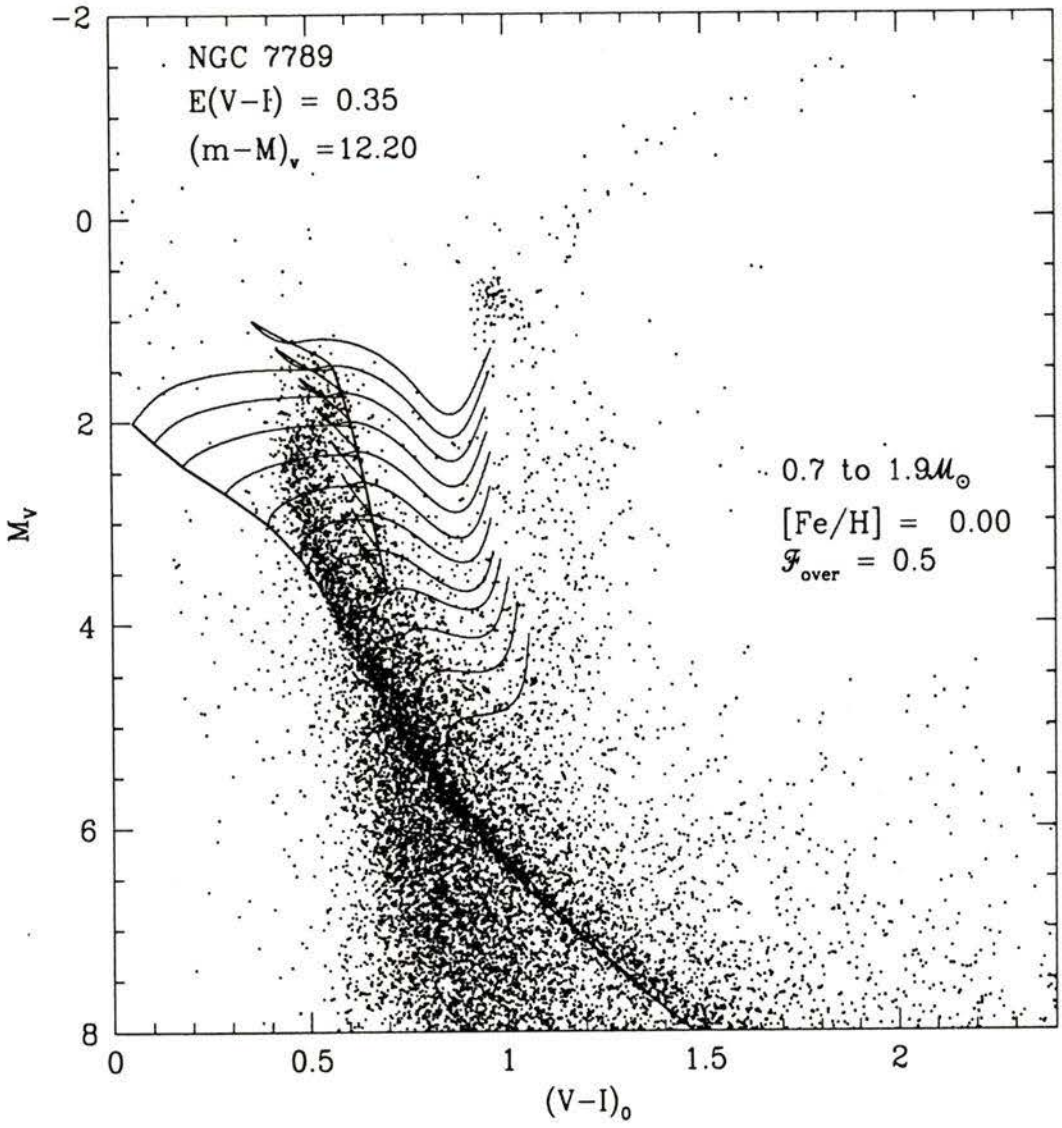

Figure 3.12: Similar to Fig. 3.10 except that the adopted distance modulus is reduced by 0.2 mag and the reddening is adjusted accordingly. The models are calculated with an intermediate amount of overshooting and the TAMS agrees with the observed one.

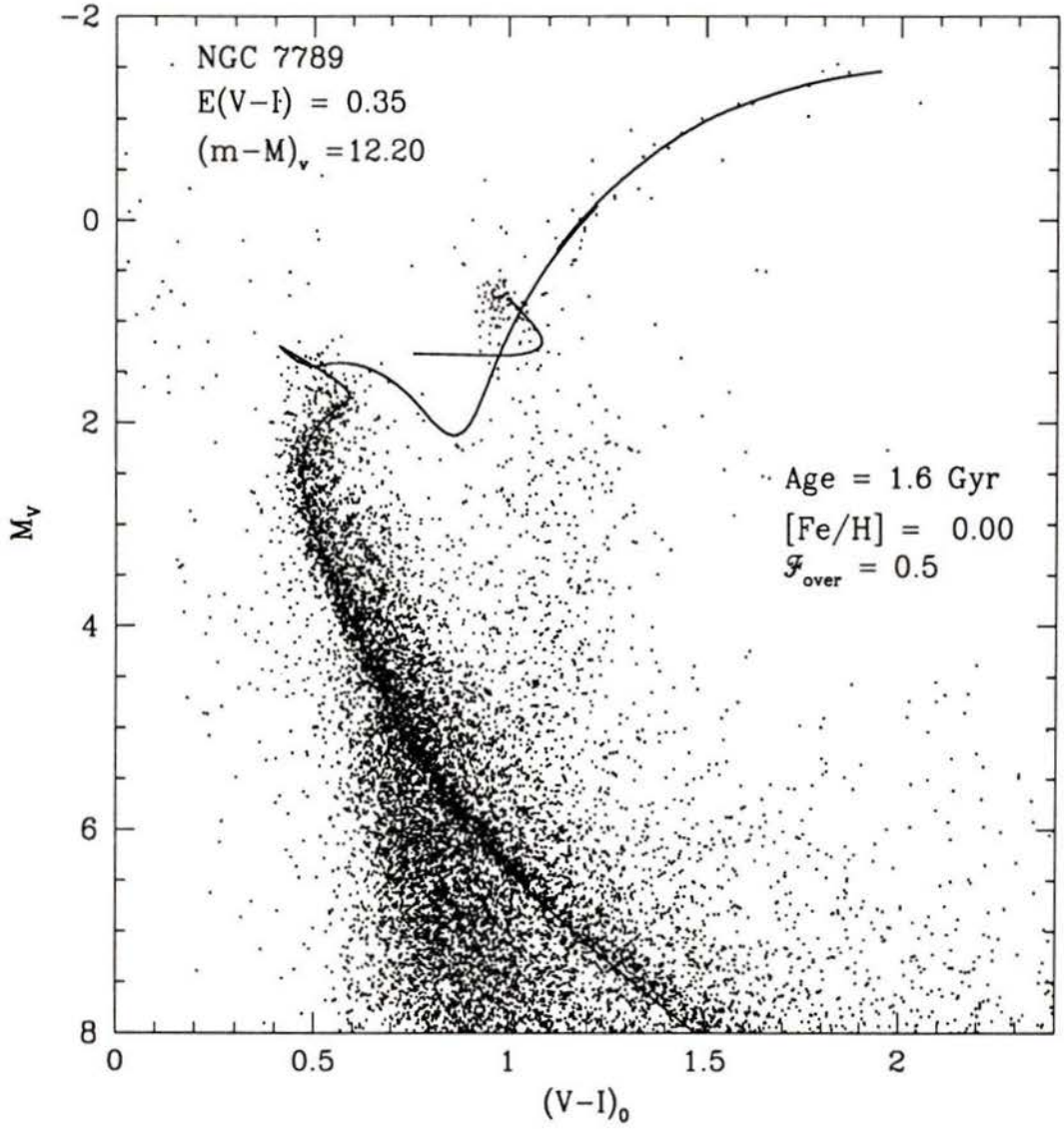

Figure 3.13: CMD for NGC 7789 with an isochrone for 1.6 Gyr superimposed, along with its corresponding theoretical ZAHB.

transition mass, is much lower than the values found in non-overshooting models. For instance, a $1.7\mathcal{M}_\odot$ star having solar abundances is predicted to have $\mathcal{M}_c = 0.4659\mathcal{M}_\odot$ if $\mathcal{F}_{\rm over} = 0.0$ (no overshooting) versus $0.4358\mathcal{M}_\odot$ if $\mathcal{F}_{\rm over} = 0.5$. This reduction in the core mass causes a decrease of ≈ 0.3 mag in the luminosity of the ZAHB. Thus, in all clusters whose upper main-sequence stars burn hydrogen in convective cores, the theoretical ZAHB locus depends quite sensitively on the amount of core overshooting which is assumed to occur in the main-sequence phase. This is clearly an important complication in the interpretation of star cluster CMDs, particularly if $\mathcal{F}_{\rm over}$ varies with mass.

But, regardless of whether or not the ZAHB in Fig. 3.13 is somewhat too faint (due, perhaps, to a problem with the models), there also seems to be a bit of a mismatch between the predicted and observed colors of the clump stars. While it is always very risky to try to draw conclusions from color information, the assumption of a constant reddening may be partly responsible. As Twarog et al. (1997; see references therein) have noted, when the reddening is substantial, a red giant will exhibit a smaller $E(B-V)$ than a hotter main-sequence star if both are obscured by the same dust layer. They suggest that the reddening correction applied to the NGC 7789 giants should be about 0.03 mag smaller than the value applied to its turnoff stars. Such a differential correction would go in the right direction to improve the agreement between the models and the observed clump (while worsening slightly the fit to the brightest giants).

Reasonably good fits of isochrones to the NGC 7789 CMD can be obtained on the assumption of smaller distances, with consequent modest in-

creases in the inferred age — e.g., 1.9 Gyr if $(m - M)_V = 11.9$ — but, if the apparent distance modulus is less than 12.0, then the predicted giant branch is well to the blue of its observational counterpart. The main argument that we can offer against the possibility that such discrepancies are due to inadequacies in the adopted color transformations, is that the same models produce a superb match to the CMD of NGC 6819 (see Rosvick and VandenBerg, 1998), which is only 0.6–0.9 Gyr older than NGC 7789. Pending further developments, we therefore believe that Fig. 3.13 portrays the best interpretation of the NGC 7789 photometry *if* this cluster has the same chemical composition as the Sun.

We now turn to the possibility that it has [Fe/H] = −0.2, which is more consistent with the available metallicity determinations. By adopting various choices for the apparent distance modulus and examining the best-fit isochrone for that distance, it quickly became evident that $(m - M)_V$ had to be $\lesssim 12.15$ in order for the giant branch of the corresponding isochrone to be at least as long as the observed one. The isochrone fit that we obtained to the NGC 7789 photometry on the assumption of this distance upper-limit is shown in Figure 3.14: the inferred age is 1.7 Gyr. Except for the giant branch, the fit is quite comparable to that given in Fig. 3.13. If anything, the predicted ZAHB magnitudes agree slightly better with those of the observed clump, though a modest color offset (0.05 mag, say) remains. As before, a value of $\mathcal{F}_{\rm over} = 0.5$ yields good agreement between the predicted and observed TAMS. (This is sufficiently clear in Fig. 3.14 that we decided not to include a plot, like Fig. 3.12, which compares evolutionary tracks with the observed CMD.)

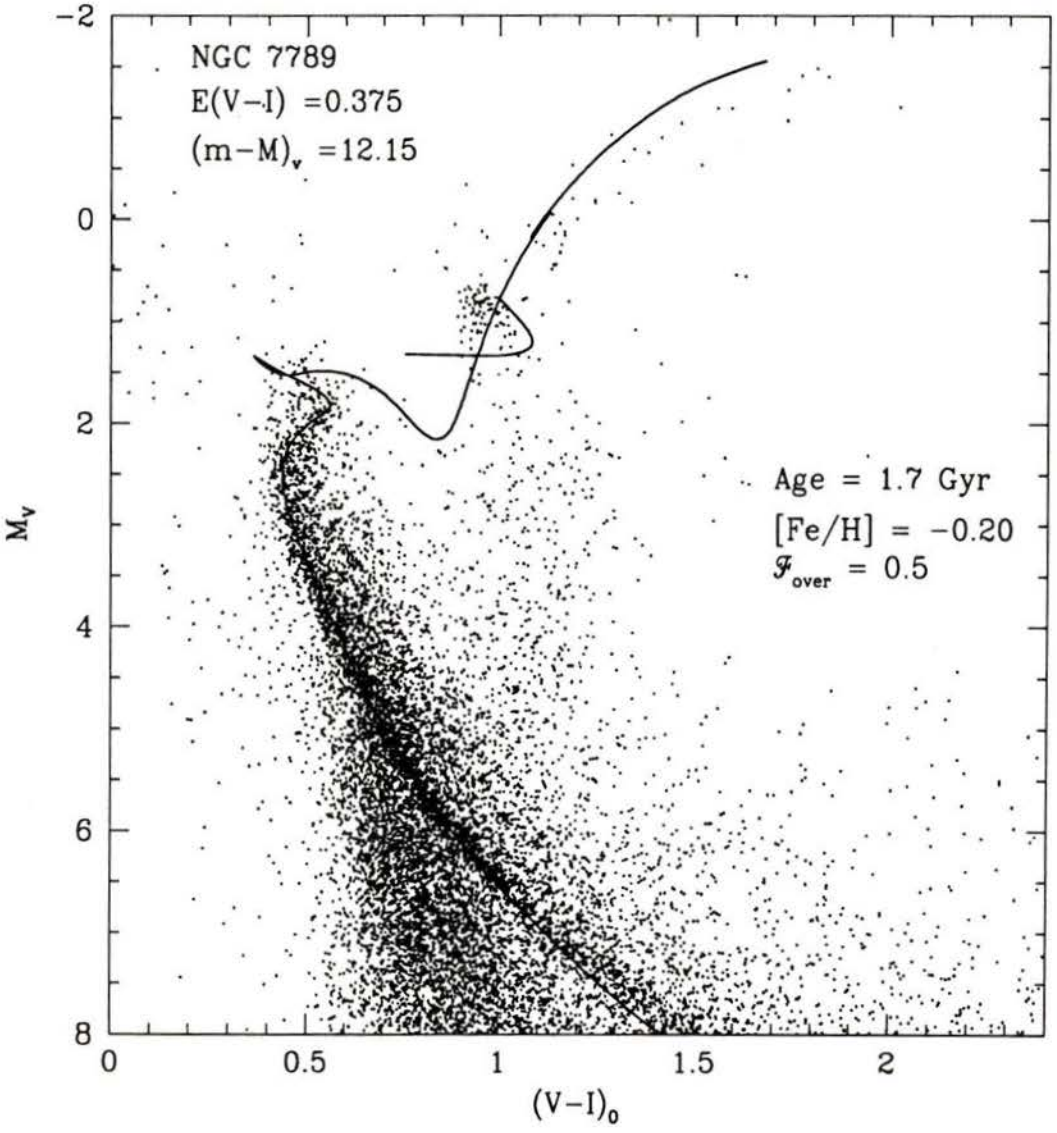

Figure 3.14: CMD for NGC 7789 with a 1.7 Gyr isochrone for [Fe/H] = −0.2 superimposed.

Because of the giant branch discrepancy, it is tempting to conclude that [Fe/H] = −0.2 is too low. Obviously, much more work is needed to better establish the reliability of the models before such an inference could be taken seriously, though, in support of this possibility, we note that Twarog et al. (1997) recently derived [Fe/H] = −0.08 from DDO photometry. What is fortunate is that the derived value of $\mathcal{F}_{\rm over}$ as well as the inferred distance and age are only weakly dependent on the cluster metallicity. Thus, regardless of which value of [Fe/H], in the range $-0.2 \leq$ [Fe/H] ≤ 0.0, applies to NGC 7789, it seems clear that the models must assume a value of $\mathcal{F}_{\rm over}$ close to 0.5 in order to match the observed CMD in the vicinity of the turnoff, that the cluster distance is approximately $(m - M)_V = 12.2$, and that the age of NGC 7789 is 1.6–1.7 Gyr.

3.3 Radial velocities of giants

Member stars are subdivided into three groups in this study: members with constant velocity (MC), members with variable radial velocity (MV), and members with one or no radial velocity data measurements in the present study (M). Fifty-three stars are classed MC based on $P(\chi^2) \geq 0.01$ and the proper motion membership probability $P(\mu) > 80\%$. Twenty-five stars are classified as MV because they have $P(\chi^2) < 0.01$ (which means that their errors come from a non-random source with 99% confidence) and because they have $P(\mu) > 80\%$. Although K977 has $P(\mu) = 0\%$, it is classified MV because of its location on the CMD giant branch, and its mean velocity in the present study, which is consistent with that of the cluster. Eleven stars with only one observation are also taken as members (M). All these stars

have $P(\mu) > 70\%$ and their velocities are within 4.7σ of the mean cluster velocity. Three of them are considered radial velocity members by Scott et al. (1995).

Seventeen stars are classified non-members (NM) since they have $P(\chi^2) > 0.01$ and $P(\mu) < 50\%$. These stars are all lie over 7.1σ away from the mean cluster velocity. One NM star, K1149, has variable radial velocity. Four of our NM stars were also considered non-members by Scott et al., while two others were classified as members on the basis of radial-velocities in that study.

Membership estimates for six stars are classified as uncertain (U). M1244 is a non-member star by $P(\mu) = 2\%$, but its velocity from the present study is consistent with the cluster mean. Five other stars (K193, K605, K859, M125 and M748) have velocities from the present study that are more than 6.6σ away from the mean cluster velocity, but they are considered proper motion members by McNamara and Solomon (1981) or radial velocity members by Scott et al. (1995).

3.3.1 The mean cluster velocity and its dispersion

The mean cluster velocity and its dispersion were calculated for stars after excluding stars whose velocity is deviant by more than 2σ. Stars excluded are constant velocity members (MC) K526, K692 and K1114, and variable velocity members (MV) K160, K489, K491, K865 and K897. The mean cluster velocity is -54.92 km s^{-1} and its dispersion is 0.86 km s^{-1} based on 50 MC stars. The dispersion increases to 1.20 km s^{-1} when 20 MV stars are included, while the mean velocity changes very little to -54.77 km s^{-1}. We adopted,

therefore, a mean cluster velocity for NGC 7789 of -54.9 ± 0.12 km s^{-1} and a dispersion of 0.86 km s^{-1}. Fig. 3.15 shows the radial velocities as a function of the distance from the cluster center for the 53 MC members and 25 MV members, with the adopted mean cluster velocity and the dispersion indicated by a heavy line and error bars.

Inspection of Fig. 3.15 suggests that outside a radius of 8 arcmin the radial velocity dispersion is considerably lower than it is interior to that radius. If this result is correct, it is possibly due to the presence of binaries of very long period preferentially in the central area of the cluster.

Below we summarise previous determinations of the mean cluster velocity.

- Stryker and Hrivnak (1984) found that the mean radial velocity of NGC 7789 is -54 km s^{-1} from three giants, K319, K415, K489, during a study of the radial velocity variations in the blue stragglers from image-tube spectra at a dispersion of 30 Å mm^{-1}. K319 was noticed to be a velocity variable, which is confirmed by our observations, while we demonstrate that K489 is also a velocity variable.

- Moderate-resolution spectroscopic observations (Friel et al., 1989), with an accuracy of 10 km s^{-1}, for 12 NGC 7789 giants gave a mean cluster velocity of -57 ± 7 km s^{-1}. Our study indicates that four of their stars (K491, K637, K737, K977) are probable velocity variables. It is interesting that their result and ours are similar for K605 and K859, for which we don't give any membership assessment since the velocity of K605 is too high and our observational errors for K859 are too large.

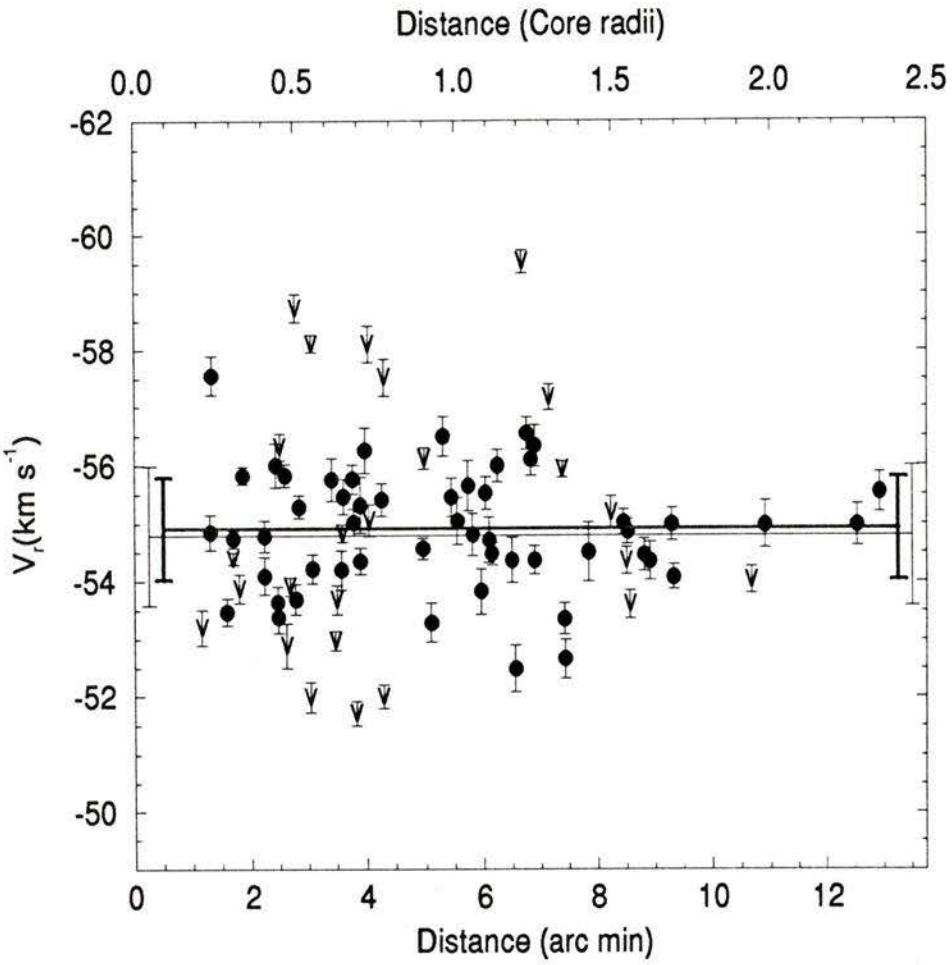

Figure 3.15: Mean radial velocity as a function of the angular distance from the center of the cluster. Note that the core radius of NGC 7789 is 5.′5. *Solid circles*: 53 members with constant radial velocities, "V" symbols: 25 members with variable radial velocities. The standard deviation of the individual velocities is shown for each star. The *thick solid line* indicates the mean cluster velocity, -54.92 ± 0.12 km s^{-1}, with the standard deviation shown at each end, $\pm$ 0.86 km s^{-1}. This is calculated from only stars with constant radial velocities. The *thin line* shows the same values determined for members with both constant and variable velocities: -54.79 ± 0.14 km s^{-1} and 1.20 km s^{-1}.

- Recently, Scott et al. (1995) determined a mean cluster velocity of -64 km s^{-1} for NGC 7789 from spectroscopic observations of 49 member giants with about ± 10 km s^{-1} accuracy. However, they adopted -57 km s^{-1} for their kinematic study in open clusters after considering their low accuracy and comparing with the results of Friel et al. (1989) and with the unpublished data of Hesser and McClure, which were the preliminary results of the present paper.

3.3.2 The radial velocity variables

The sparse data sampling for most of the stars, even with an observation baseline extending up to 6000 days, makes it difficult to determine orbital elements. With a 99% confidence level that errors are non-random, 25 stars are identified as probable radial-velocity variable stars. The ratio of external and internal errors, E/I, of 20 of those stars is more than 2, considered as the minimum value for variability in past studies (e.g., Stryker and Hrivnak, 1984). The remaining five have E/I $>$ 1.6. Assuming all MV stars are binaries, the overall binary frequency is 32% (25/78), which is similar to the mean binary frequency, 25% to 50%, from previous studies of open clusters, as mentioned in chapter 1.

Several spectroscopic studies of globular-cluster giants have shown that more velocity variability is found among stars near the tip of red giant branch than for stars with fainter magnitudes. This is believed to arise from convective or pulsational motion in their atmosphere (Pryor et al., 1988; Côté et al., 1996). However, such a trend is not found in our data for NGC 7789.

3.3.3 The apparent distribution of red giants of radial velocity variables

Mass segregation during the dynamical evolution of clusters has been predicted by numerical simulations (Spitzer and Mathieu, 1980), and confirmed by several studies of the radial distribution of stars with different masses (Latham, 1985; Abt, 1980). The cumulative distribution of stars in NGC 7789 with constant velocity and with variable velocity is shown in Fig. 3.16. Although the variable stars appear to be more centrally concentrated, as expected if they are binaries of higher total masses than single stars, a Kolmogorov-Smirnov test gives a probability of only 85% that the distributions of stars with constant radial velocity (presumably single stars) and with variable radial velocity (presumably binaries) are different. Note, however, that with an age $log\ t = 9.13$ (Carraro and Chiosi, 1994), NGC 7789 would fall in the second group of three open clusters considered in a similar analysis by Raboud and Mermilliod (1994). They found the difference to be significant at the 87.9% level. Taken together, the joint probability that the apparent radial segregation of spectroscopic binaries is due to chance is of order $15\% \times 12\% \approx 2\%$. Therefore, the combined data for NGC 7789 (present study) and NGC 2362, 2477, 6940 (Raboud and Mermilliod, 1994) show mass segregation at the 98% confidence level.

3.3.4 Color-magnitude diagram of the red giants in NGC 7789

In the CMD of the red giants in NGC 7789 (Fig. 3.17), the distribution of stars in the well-defined clump and upper giant branch is shown with different

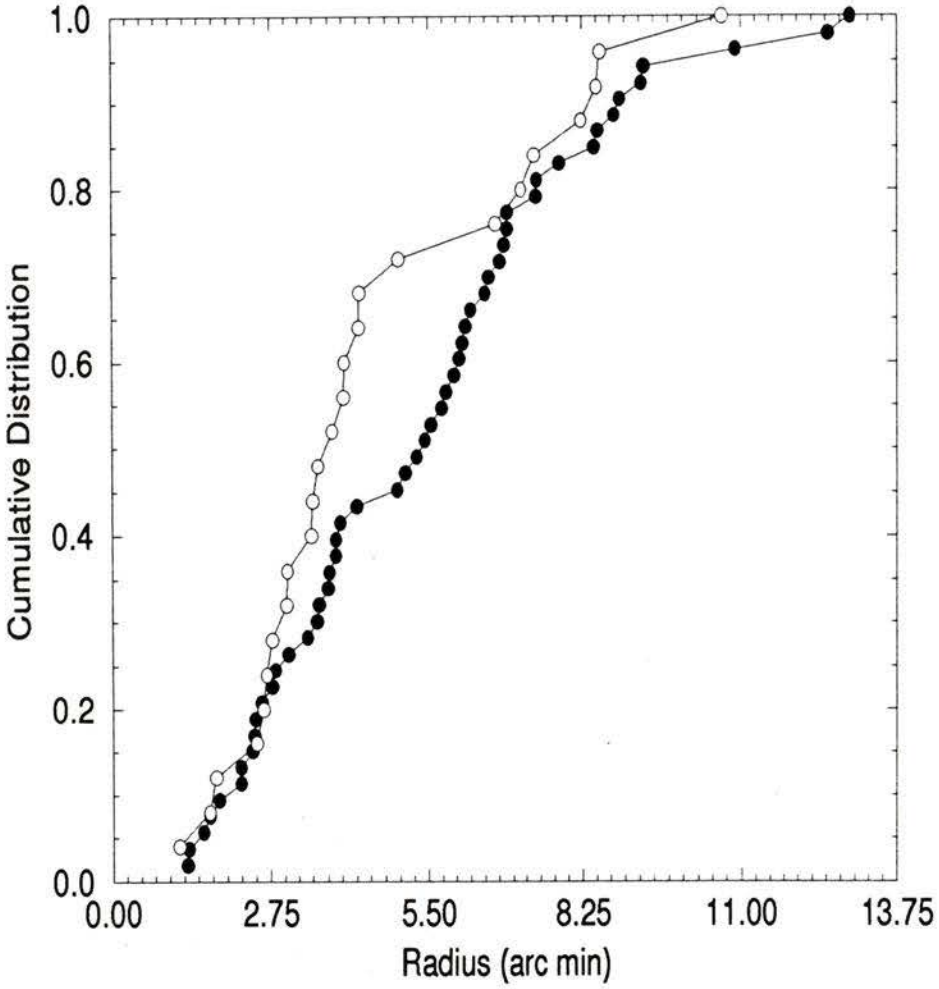

Figure 3.16: The cumulative radial distribution of stars with constant radial velocity (*solid circles*, 53 stars) and with variable radial velocity (*open circles*, 23 stars) in NGC 7789. The two distributions show an apparent central concentration of radial velocity variables relative to that of stars with constant radial velocity.

symbols depending on their membership. To compare the ratio of radial-velocity variables for different populations, the clump stars are considered to have colors $1.25 < (V-I) < 1.4$ and magnitude $12.8 < V < 13.4$, while upper giant-branch stars are considered to be all stars which have $(V-I) > 1.2$ and $V < 13.4$ excluding the clump stars. The frequency of radial-velocity variables for the member clump stars and the upper giants is almost identical (29% for the clump stars and 28% among the upper giants).

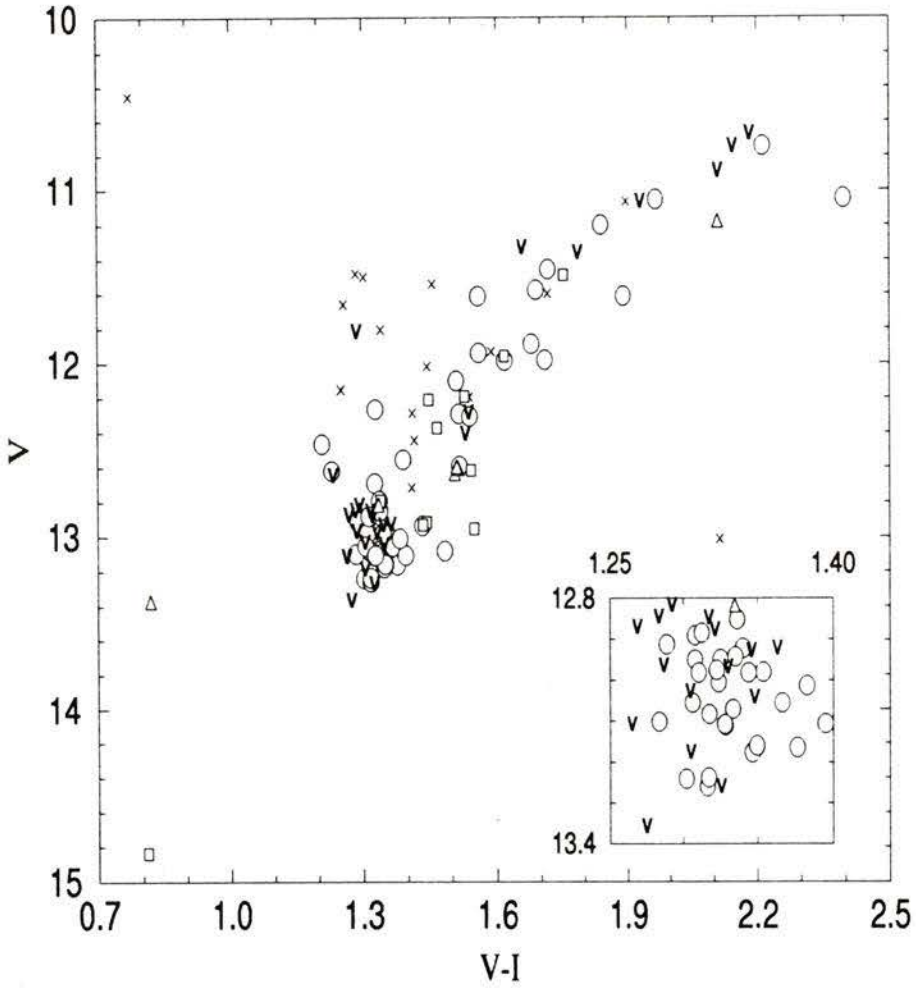

Figure 3.17: Color-magnitude diagram of the red giants in NGC 7789. *Open circles*: 53 red giant members with constant radial velocity (MC), "V" marks: 25 radial-velocity variable members (MV), *squares*: 11 members with one radial velocity data (M), *open triangles*: 6 stars with uncertain membership (U), *crosses*: 17 non-members (NM). The clump star region is shown on the inset box with the expanded scale.

Chapter 4

Summary

4.1 Photometry

We have presented extensive CCD photometry in V and I for the open cluster NGC 7789 that establishes its fiducial sequences on the $(V, V-I)$–plane down to $V \sim 21$ ($M_V \sim 9$). Despite the relatively high $E(V-I) \approx 0.35$, these sequences are very tight and well-defined, indicating that the reddening is nearly constant across the face of the cluster. A confrontation of these data with modern stellar evolutionary models has demonstrated, beyond any doubt, that significant convective core overshooting must occur in the main sequence phase. Non-overshooting models are unable to match either the observed morphology in the vicinity of the turnoff or the location of the TAMS relative to that of the main sequence. Perhaps the most novel aspect of our analysis is that the length of the red-giant branch has been used to set a lower limit to the cluster age (1.6 Gyr) and an upper limit to its distance [$(m-M)_V = 12.2$]. An important, well-known consequence of convective core overshooting is to reduce the maximum mass of stars that undergo the helium flash: above this limit, helium-burning is ignited quiescently and extended

giant branches are not produced. As NGC 7789 has a well-developed, but not fully extended RGB, its giants must be just slightly below the lower mass limit where non-violent ignition of helium takes place.

Interestingly, we have found that the amount of overshooting that is needed to explain the NGC 7789 CMD is very similar to that inferred by Rosvick and VandenBerg (1998) for NGC 6819, despite the fact that the two clusters differ in age by $\sim$ 1 Gyr. This suggests that the extent of overshooting does not depend sensitively on the turnoff mass at least in the age range encompassed by these two clusters.

4.2 Radial Velocities of giants

Radial-velocity observations for 112 giant stars in NGC 7789 observed since 1979 at the Dominion Astrophysical Observatory were used to determine cluster membership and their radial-velocity duplicity was determined based on statistical analysis. Seventy-eight cluster members were selected on the basis of radial velocities and proper motions (McNamara and Solomon, 1981). Among these, 25 stars (32%) are considered to be radial-velocity variables. The cluster mean velocity was found to be -54.9 ± 0.12 km s^{-1} and its dispersion 0.86 km s^{-1} using 47 stars with constant velocity. Twelve additional stars with one RVS observation were also selected as members on the basis of both their radial velocities and their proper motions. Overall a frequency of 32% for radial-velocity variables is consistent with that published for other clusters. The binary frequency for the more luminous giants and clump stars is similar. The radial-velocity variables seem to be slightly more concentrated toward the center than stars with constant velocity. When taken alone, this

result is significant only at the 85% level. However, three additional clusters of the same approximate age studied by Raboud and Mermilliod (1994) show the same effect, which strongly suggests that mass segregation is being detected in these four clusters. More observations are needed to obtain orbital elements for the stars which have variable radial velocities.

Bibliography

Abt, H.: 1980, *Astrophys. J.* **241**, 275

Abt, H. and Willmarth, D.: 1996, in E. Milone and J.-C. Mermilliod (eds.), *The Origins, Evolution, and Destinies of Binary Stars in Clusters*, ASP Conf. Ser. 90, p. 105

Anthony-Twarog, B., Twarog, B., Kaluzny, J., and Shara, M.: 1990, *Astron. J.* **99**, 1504

Arp, H.: 1962, *Astrophys. J.* **136**, 66

Barbaro, G. and Pigatto, L.: 1984, *Astron. & Astrophys.* **136**, 355

Bergbusch, P. and VandenBerg, D.: 1992, *Astrophys. J. Supp.* **81**, 163

Bergbusch, P. and VandenBerg, D.: 1998, in preparation

Bertelli, G., Bressan, A., Chiosi, C., and Angerer, K.: 1986, *Astron. & Astrophys. Supp.* **66**, 191

Breger, M.: 1982, *Astrophys. J.* **263**, 199

Breger, M. and Wheeler, J.: 1980, *Publ. Astron. Soc. Pacific* **92**, 514

Burbidge, E. and Sandage, A.: 1958, *Astrophys. J.* **128**, 174

Canterna, R., Geisler, D., Harris, H., and Olszewski, E.: 1986, *Astron. J.* **92**, 79

Canuto, V. and Christensen-Dalsgaard, J.: 1998, *Ann. Rev. Fluid Mech.* **30**, 167

Carraro, G. and Chiosi, C.: 1994, *Astron. & Astrophys.* **287**, 761

Clariá, J.: 1979, *Astron. Space Sci.* **66**, 201

Coleman, L.: 1982, *Astron. J.* **87**, 369

Côté, P., Pryor, C., McClure, R., Fletcher, J., and Hesser, J.: 1996, *Astron. J.* **112**, 574

Daniel, S., Latham, D., Mathieu, R., and Twarog: 1994, *Publ. Astron. Soc. Pacific* **106**, 281

Davis, L.: 1992, Private communication

Demarque, P. and Hirshfeld, A.: 1975, *Astrophys. J.* **202**, 346

Demarque, P., Sarajedini, A., and Guo, X.-J.: 1994, *Astrophys. J.* **426**, 165

Drilling, J. and Schönberner, D.: 1987, in A. Philip, J.W., D. Hayes, and J. Liebert (eds.), *The Second Conference on Faint Blue Stars, IAU Coll. 95*, p. 587, L. Davis Press

Fletcher, J., Harris, H., McClure, R., and Scarfe, C.: 1982, *Publ. Astron. Soc. Pacific* **94**, 1017

Friel, E. and Janes, K.: 1993, *Astron. & Astrophys.* **267**, 75

Friel, E., Liu, T., and Janes, K.: 1989, *Publ. Astron. Soc. Pacific* **101**, 1105

Gilroy, K.: 1989, *Astrophys. J.* **347**, 835

Gim, M., Hesser, J., McClure, R., and Stetson, P.: 1998, *Publ. Astron. Soc. Pacific*, in press (Paper I)

Griffin, R.: 1967, *Astrophys. J.* **148**, 465

Griffin, R. and Gunn, J.: 1974, *Astrophys. J.* **191**, 545

Hobbs, L. and Thorburn, J.: 1991, *Astron. J.* **102**, 1070

Jahn, K., Kaluzny, J., and Rucinski, S.: 1995, *Astron. & Astrophys.* **295**, 101

Janes, K.: 1977, *Astron. J.* **82**, 35

Jennens, P. and Helfer, H.: 1975, *M.N.R.A.S.* **172**, 681

Küstner, F.: 1923, Bonner Veröff., No. 18

Landolt, A.: 1992, *Astron. J.* **104**, 340

Latham, D.: 1985, in A. Philip and D. Latham (eds.), *Stellar Radial Velocities*, p. 21, Schenectady, L. Davis

Manteiga, M., Martinez Roger, C., Morales, C., and Sabau, L.: 1991, *Astron. & Astrophys.* **251**, 49

Manteiga, M., Martinez Roger, C., and Pickles, A.: 1989, *Astron. Space Sci.* **156**, 169

Martinez Roger, C., Paez, E., Castellani, V., and Straniero, O.: 1994, *Astron. & Astrophys.* **290**, 62

Mayor, M.: 1985, in A. Philip and D. Latham (eds.), *Stellar Radial Velocities*, p. 35, Schenectady, L. Davis

Mazzei, P. and Pigatto, L.: 1988, *Astron. & Astrophys.* **193**, 148

McClure, R., Fletcher, J., Grundman, W., and Richardson, E.: 1985, in A. Philip and D. Latham (eds.), *Stellar Radial Velocities*, p. 49, Schenectady, L. Davis

McNamara, B.: 1980, *Publ. Astron. Soc. Pacific* **92**, 682

McNamara, B. and Solomon, S.: 1981, *Astron. & Astrophys. Supp.* **43**, 337

Mermilliod, J.-C., Anderson, J., Nordström, B., and Mayor, M.: 1995, *Astron. & Astrophys.* **299**, 53

Mermilliod, J.-C., Clariá, J., Anderson, J., and Mayor, M.: 1997, *Astron. & Astrophys.* **324**, 91

Mermilliod, J.-C., Huestamendia, G., del Rio, G., and Mayor, M.: 1996,

Astron. & Astrophys. **307**, 80

Mermilliod, J.-C. and Mayor, M.: 1989, *Astron. & Astrophys.* **219**, 125

Mermilliod, J.-C. and Mayor, M.: 1990, *Astron. & Astrophys.* **237**, 61

Milone, A. and Latham, D.: 1994, *Astron. J.* **108**, 1828

Montgomery, K., Marschall, L., and Janes, K.: 1993, *Astron. J.* **106**, 181

Nissen, P., Twarog, B., and Crawford, D.: 1987, *Astron. J.* **93**, 634

Pendl, E.: 1975, *Astron. & Astrophys.* **41**, 239

Pilachowski, C.: 1985, *Publ. Astron. Soc. Pacific* **97**, 801

Pilachowski, C.: 1986, *Astrophys. J.* **300**, 289

Pryor, C., Latham, D., and Hazen, M.: 1988, *Astron. J.* **96**, 123

Raboud, D. and Mermilliod, J.-C.: 1994, *Astron. & Astrophys.* **289**, 121

Rosvick, J. and VandenBerg, D.: 1998, *Astron. J.* **115**, 1516

Roxburgh, I.: 1978, *Astron. & Astrophys.* **65**, 281

Roxburgh, I.: 1989, *Astron. & Astrophys.* **211**, 361

Scott, J., Friel, E., and Janes, K.: 1995, *Astron. J.* **109**, 1706

Sneden, C. and Pilachowski, C.: 1986, *Astrophys. J.* **301**, 860

Spitzer, L., J. and Mathieu, R.: 1980, *Astrophys. J.* **241**, 618

Stetson, P.: 1987, *Publ. Astron. Soc. Pacific* **99**, 191

Stetson, P.: 1990, *Publ. Astron. Soc. Pacific* **102**, 932

Stetson, P.: 1994, *Publ. Astron. Soc. Pacific* **106**, 250

Stetson, P.: 1997, private communication

Strom, K. and Strom, S.: 1970, *Astrophys. J.* **162**, 523

Stryker, L. and Hrivnak, B.: 1984, *Astrophys. J.* **278**, 215

Sweigart, A., Greggio, L., and Renzini, A.: 1989, *Astrophys. J. Supp.* **69**, 911

Thogerson, E., Friel, E., and Fallon, B.: 1993, *Publ. Astron. Soc. Pacific* **105**, 1253

Twarog, B., Ashman, K., and Anthony-Twarog, B.: 1997, *Astron. J.* **114**, 2556

Twarog, B. and Tyson, N.: 1985, *Astron. J.* **90**, 1247

Appendix A

The radial-velocity observational data

Appendix A gives the Julian date, radial velocity and internal error for each star. For the analysis in this study, we have omitted seventeen obervations with error $\geq$ 1.0 km s^{-1} and three other observations which seem to be dubious. Data marked *a* and *b* in Table A.1 are unused for further analysis in this thesis because of either *Errors* $>$ 1.0 km s^{-1} or that the quality was deemed to be dubious.

Table A.1: RVS Data

Name			Name			Name		
JD	Vel.	Err.	JD	Vel.	Err.	JD	Vel.	Err.
K57			49269.876	−62.59	0.44	**K248**		
46392.834	−54.00	0.72	50344.796	−62.11	0.57	46035.742	−54.35	0.39
K72			**K193**			**K254**		
45975.986	−53.33	0.23	46037.770	−61.40	0.50	45975.852	−56.47	0.33
46035.770	−54.69	0.26	47444.871	−59.87	1.05[a]	47444.938	−56.80	0.95
46296.990	−54.57	0.34	47444.876	−62.15	0.52	47444.944	−56.78	0.77
46380.870	−54.94	0.81	48508.963	−62.00	0.57	48544.917	−56.29	0.50
47444.959	−53.97	0.47	49269.904	−60.58	0.46			
49994.911	−52.75	0.49	50277.930	−61.47	0.40	**K255**		
50276.832	−54.57	0.36				45962.897	−53.25	0.34
			K200			46035.727	−55.03	0.39
K80			45618.691	−55.03	···	46383.815	−52.93	0.58
45618.730	−51.75	···	45972.834	−56.08	0.55	48508.928	−54.89	0.71
45972.814	−55.37	0.32	46295.959	−56.03	0.34	48508.928	−55.12	0.63
45995.942	−54.88	0.80				48508.936	−55.47	0.54
46035.777	−54.15	0.55	**K212**			48544.931	−54.57	0.88
46295.973	−53.93	0.73	45990.791	−54.92	0.35			
47081.875	−52.89	0.93	46110.726	−54.03	0.84	**K297**		
49269.888	−52.48	1.06[a]	46295.983	−54.98	0.44	45975.950	−63.72	0.44
50344.815	−54.84	0.58	47444.953	−54.73	2.52[a]	46037.797	−63.93	0.50
						46383.852	−54.68	0.58
K152			**K232**			47444.862	−49.68	0.58
50127.666	−54.53	0.65	45990.806	−54.37	0.35	47444.865	−50.19	0.62
50276.889	−55.18	0.41	46037.785	−54.82	0.52	48508.978	−52.34	0.70
50313.810	−55.03	0.42	47444.886	−53.82	0.56	48544.907	−54.67	0.50
			49269.937	−54.39	0.80	49269.919	−57.03	0.82
K160						50278.827	−61.67	0.48
45618.715	−57.58	···	**K244**					
45972.824	−59.70	0.45	46052.728	−52.16	0.53	**K301**		
46295.968	−56.38	0.38	47444.902	−53.27	0.84	45975.909	−52.11	0.50
47081.854	−61.17	0.66	47444.911	−54.21	0.55	45992.752	−53.10	0.45
47444.897	−61.39	0.64	48544.924	−53.49	0.43	46035.762	−55.39	0.43

Table A.1: *Continued*

Name			Name			Name		
JD	Vel.	Err.	JD	Vel.	Err.	JD	Vel.	Err.
45992.752	−53.10	0.45	46383.787	−53.65	0.73	46294.977	−56.65	0.33
46035.762	−55.39	0.43	47444.856	−53.68	0.57	46383.722	−50.85	0.63
46380.847	−53.71	0.60				47029.985	−52.52	0.74
46711.820	−54.49	0.67	**K327**			47081.931	−56.80	0.34
47081.839	−52.96	0.49	45992.836	−54.74	0.39	47950.655	−55.34	0.45
48508.886	−53.76	1.08[a]	46035.703	−58.19	0.76	48130.965	−52.13	0.51
50128.627	−55.48	0.58	46394.599	−56.44	0.80	48544.844	−50.65	0.58
50344.855	−55.18	0.48	46768.755	−56.71	0.53	48950.742	−50.86	0.62
			48544.871	−56.15	0.88	48950.750	−50.26	0.47
K304			50031.870	−56.77	0.85	49269.856	−58.38	0.64
50316.934	−13.13	0.49	50301.819	−54.42	0.74	49994.973	−55.76	0.60
50361.739	−13.04	0.38				50031.808	−52.42	0.80
50365.724	−12.76	0.50	**K329**			50277.800	−50.03	0.30
			45618.668	−54.39	...			
K310			45972.840	−55.31	0.49	**K347**		
48508.891	−52.74	0.71	46295.947	−54.59	0.43	45606.902	−54.72	...
			46394.670	−55.42	0.77	45972.861	−56.04	0.52
K312			47029.992	−54.37	1.03[a]	46383.751	−55.61	0.58
45669.898	−58.34	...[b]	48130.970	−53.53	0.62	46768.734	−57.35	0.46
46035.719	−14.90	0.62	49269.864	−53.84	0.60	47444.926	−56.48	0.46
47445.982	−12.96	0.58	50344.927	−53.58	0.42			
48544.879	−12.65	0.55				**K348**		
50301.915	−11.38	0.59	**K337**			45669.855	−52.37	...
			45669.879	−35.06	0.00	45972.872	−54.03	0.49
K319			46035.695	−37.20	0.46	46394.627	−54.38	0.60
45960.873	−43.34	0.35	48508.910	−36.33	0.40	46712.913	−54.49	0.82
45992.810	−63.91	0.65	48508.910	−36.60	0.38	48508.900	−53.98	0.60
46037.824	−76.66	0.77	48544.882	−35.85	0.48			
46380.669	−52.83	0.81	48950.820	−35.43	0.71	**K353**		
47081.898	−60.03	0.78	50344.707	−35.74	0.38	45618.676	−54.52	...
47950.671	−50.00	2.03[a]				45972.879	−56.62	0.42
49269.816	−75.17	0.96	**K338**			46295.952	−54.20	0.54
			45612.789	−58.87	...	46394.682	−54.91	0.55
K321			45972.849	−54.35	0.30	48130.974	−55.78	0.56
45990.821	−54.02	0.42	46035.828	−60.32	0.33	50361.861	−54.61	0.43

Table A.1: *Continued*

Name			Name			Name		
JD	Vel.	Err.	JD	Vel.	Err.	JD	Vel.	Err.
			48508.869	−54.67	0.61	48130.999	−54.96	0.77
K415			48950.729	−54.62	0.66			
45618.738	−51.39	···	49269.770	−54.14	0.37	**K489**		
45972.885	−54.30	0.42	49995.909	−53.08	0.53	45976.002	−43.76	0.42
45995.774	−53.00	0.35	50018.993	−51.08	0.88	45992.902	−47.71	0.31
46037.809	−53.59	0.35	50301.961	−53.84	0.52	46037.844	−58.23	0.55
46383.773	−52.32	0.39	50316.760	−55.63	0.39	46052.875	−61.03	0.49
46712.862	−52.08	0.45				46093.785	−64.49	0.48
48130.978	−53.50	0.52	**K466**			46100.809	−66.09	0.78
49994.854	−52.72	0.21	45606.931	−47.07	···	46380.643	−60.38	0.59
50031.745	−54.75	0.44	46110.708	−48.06	0.55	46768.700	−45.90	0.46
50278.946	−54.22	0.44	47445.992	−48.23	0.39	47029.999	−64.35	0.41
			48544.862	−49.53	0.68	47081.944	−62.87	0.26
K416			48950.724	−48.35	0.52	48544.851	−66.03	0.45
45618.660	−53.65	···	49269.794	−48.97	0.56	48950.718	−46.81	0.43
45972.890	−54.68	0.45	50344.696	−48.57	0.42	49269.781	−65.93	0.50
46712.895	−52.95	0.83				50018.933	−61.59	0.50
48130.942	−53.75	0.70	**K468**			50031.764	−64.23	0.57
48544.838	−52.92	0.43	45618.652	−55.42	···	50274.919	−61.62	0.53
			45622.761	−57.22	···			
K444			46294.970	−55.79	0.30	**K491**		
45607.007	−52.60	···	46712.829	−55.35	0.51	45992.862	−66.21	0.44
45972.897	−54.47	0.50	47081.821	−56.04	0.36	48130.988	−54.55	0.67
46383.890	−54.49	0.77	47444.831	−54.83	0.56	48544.889	−55.77	0.59
46712.878	−53.62	0.72	48130.936	−56.43	0.63	48950.766	−54.78	0.80
48130.957	−53.76	0.71	48157.873	−55.78	0.34	50344.909	−53.97	0.58
			48544.828	−55.92	0.30			
K461			49269.761	−55.98	0.59	**K494**		
44191.840	−51.96	···	49994.701	−55.28	0.30	44178.020	−56.95	···
45962.884	−54.19	0.33	50301.941	−54.70	0.46	45963.006	−53.92	0.25
46052.885	−54.55	0.40				45995.757	−53.54	0.35
46380.881	−55.15	0.39	**K476**			46037.836	−55.76	0.32
46711.811	−54.04	0.44	45990.834	−54.65	0.51	46052.631	−54.12	0.31
47081.825	−54.58	0.63	46712.845	−56.22	0.81	46100.801	−54.43	0.38
47444.838	−53.97	0.50	47444.843	−54.74	0.76	46294.959	−54.91	0.33

Table A.1: *Continued*

Name			Name			Name		
JD	Vel.	Err.	JD	Vel.	Err.	JD	Vel.	Err.
46380.634	−55.19	0.45	46712.822	−54.98	0.61			
46419.702	−53.95	0.40	47029.977	−55.83	0.60		**K593**	
46711.807	−53.25	0.59	47444.832	−54.81	0.53	45970.847	−55.61	0.54
47029.972	−54.82	0.49	47444.835	−54.34	0.66	45990.863	−56.76	0.50
47081.818	−53.38	0.40	47950.640	−54.05	0.50	46419.730	−57.28	0.70
47444.828	−53.76	0.45	48130.950	−54.71	0.30	46711.945	−55.74	0.68
47950.634	−53.92	0.41	49269.848	−55.45	0.41			
48130.933	−54.48	0.33	49994.739	−54.46	0.70		**K601**	
48157.870	−53.86	0.35	50276.947	−55.62	0.26	50387.727	−50.92	0.39
48508.865	−54.57	0.43						
48544.825	−54.62	0.42		**K526**			**K605**	
48950.712	−53.70	0.75	45990.852	−52.67	0.39	45606.943	−48.61	...
49269.754	−52.66	0.59	46053.828	−52.90	0.78	45970.854	−49.33	0.45
49995.834	−54.89	0.81	47444.848	−51.74	0.72	46419.754	−50.30	0.58
49995.932	−55.53	0.55				50365.761	−50.26	0.85
50018.902	−52.40	0.86		**K549**				
50030.851	−52.58	0.67	45992.920	−54.39	0.41		**K626**	
50031.717	−54.94	0.46	46383.913	−54.24	0.58	45962.915	−53.73	0.35
50037.598	−53.05	0.54	47446.004	−53.88	0.56	46037.852	−55.80	0.45
50107.619	−53.44	0.57	48544.855	−54.26	0.42	46052.858	−55.43	0.44
50107.666	−53.69	0.76	49269.803	−53.02	0.58	46380.702	−55.81	0.84
50274.866	−54.17	0.24	50344.937	−52.34	0.44	46711.926	−53.24	0.37
50276.816	−54.09	0.37				48157.878	−54.65	0.63
50312.948	−55.67	0.88		**K555**		50301.872	−53.11	0.49
50316.746	−55.96	0.38	45612.797	−55.84	...			
50361.658	−54.09	0.38	45970.839	−55.44	0.50		**K637**	
50386.895	−54.05	0.41	46419.745	−55.40	0.53	45970.865	−43.61	0.48
50410.802	−54.04	0.46	46711.960	−53.88	0.64	45995.970	−45.45	2.08[a]
						46053.633	−47.41	0.44
	K501			**K575**		46419.637	−52.59	0.78
44880.742	−54.79	...	44880.730	−54.55	0.00	46711.911	−55.76	0.58
45606.915	−54.02	...	44907.723	−55.90	...	48157.892	−55.07	0.64
45963.014	−54.43	0.32	45606.986	−54.92	...	48544.950	−58.24	0.55
46294.965	−54.29	0.27	46052.895	−55.93	0.46	50031.791	−57.86	0.68
46392.816	−56.17	0.84	50344.748	−55.70	0.38	50277.810	−61.72	0.40

Table A.1: *Continued*

Name			Name			Name		
JD	Vel.	Err.	JD	Vel.	Err.	JD	Vel.	Err.
			45606.959	−55.38	···	45993.000	−54.34	0.58
K658			45972.905	−56.71	0.37	46037.906	−56.95	0.71
45970.875	−55.24	0.57	46039.902	−59.05	0.70	46052.664	−55.77	0.52
45995.811	−54.05	0.40	46052.681	−56.22	0.55	46380.724	−55.94	0.94
46053.621	−55.39	0.53	46419.777	−56.26	0.48	48157.905	−55.75	0.94
46419.714	−55.15	0.70	46711.840	−55.90	0.48	48157.912	−55.01	0.64
46711.893	−54.84	0.62	47081.831	−55.90	0.59	50365.804	−57.31	1.18[a]
			47444.966	−55.39	0.66	50386.709	−55.04	0.71
K665			48157.924	−55.33	0.43			
45970.891	−55.82	0.37	48950.832	−58.09	0.75	**K716**		
46419.829	−56.89	0.62	50344.762	−55.89	0.38	45712.639	−54.82	···
48157.919	−56.49	0.73				45972.915	−55.42	0.49
			K684			46053.609	−54.77	0.43
K669			45970.913	−55.98	0.47	48157.896	−53.70	0.67
44907.805	−54.22	···	46419.794	−55.08	0.71			
45606.972	−54.72	···	46711.861	−56.55	0.47	**K724**		
46052.639	−55.22	0.42				46037.863	−59.77	0.76
46383.942	−54.61	0.86	**K692**			46052.698	−57.45	0.52
46711.879	−54.72	0.47	45992.972	−57.68	0.41	46419.847	−53.38	0.66
48508.986	−54.29	0.38	46053.641	−57.79	0.44	47444.974	−50.83	0.73
48950.887	−54.25	0.66	46419.807	−57.14	0.46	48157.884	−54.86	0.68
49270.000	−53.85	0.61				48544.940	−61.75	0.68
50107.703	−54.96	0.64	**K707**			50278.913	−50.05	0.51
50316.801	−54.94	0.44	45970.930	−54.33	0.60			
			45995.788	−53.71	0.41	**K732**		
K675			46052.648	−54.19	0.49	45612.813	−52.45	···
45963.022	−53.81	0.46	46419.818	−54.33	0.57	45970.784	−54.07	0.45
46039.918	−54.92	0.47				45995.827	−53.93	0.32
46053.785	−54.24	0.56	**K709**			46053.652	−54.51	0.76
48508.991	−55.73	0.68	46039.652	−60.73	0.47	46419.857	−53.98	0.38
48950.866	−53.84	0.86	47082.011	−61.37	0.44			
49270.009	−54.13	0.54	49269.964	−60.75	0.74	**K737**		
50344.881	−53.44	0.38	50344.720	−60.91	0.47	45612.824	−51.53	···
						45972.932	−58.20	0.53
K676			**K711**			46053.664	−52.69	0.66

Table A.1: *Continued*

Name			Name			Name		
JD	Vel.	Err.	JD	Vel.	Err.	JD	Vel.	Err.
			46380.894	−56.17	0.47	48157.947	−63.19	0.44
K751			47081.998	−56.15	0.63	48544.978	−34.71	0.68
45975.973	−57.48	0.34	47444.984	−56.44	0.58			
45993.025	−56.06	0.36	47444.988	−56.02	0.51	**K859**		
46037.922	−57.33	0.40	48157.899	−55.94	0.69	45612.840	−64.75	...
46039.645	−56.48	0.47	48508.876	−55.53	0.50	46039.789	−14.96	0.92[b]
46053.813	−55.79	0.41	50107.798	−54.56	0.69	46053.734	−70.16	1.17[a]
46100.793	−55.20	0.53				46093.813	−67.30	2.19[a]
46294.990	−51.10	0.35	**K778**			48157.969	−73.40	2.15[a]
46380.744	−53.53	0.56	46039.883	−54.51	0.79	48158.023	−72.22	0.95
47082.005	−56.59	0.38	46052.757	−54.00	0.50			
48508.997	−56.89	0.43	46419.889	−53.67	0.78	**K865**		
48508.997	−57.06	0.44	47444.998	−55.61	0.75	46039.820	−62.66	0.90
48545.000	−57.27	0.38	48157.934	−53.63	0.57	46296.928	−54.72	0.45
48950.896	−52.93	0.62				47445.827	−63.10	0.42
49269.952	−54.30	0.44	**K814**			48157.987	−51.22	0.75
49994.829	−55.26	0.42	45995.906	−54.69	0.81	48545.019	−63.95	0.56
50018.916	−55.20	0.66	46039.867	−57.89	0.65	50031.849	−61.98	0.57
50031.732	−57.48	0.62	47445.793	−52.33	0.46	50277.870	−54.47	0.40
50274.751	−57.57	0.30	48157.928	−55.10	0.54			
50361.723	−57.05	0.39	48544.957	−55.95	0.92	**K866**		
			50278.855	−55.80	0.46	45612.852	−50.77	...
K752						45995.840	−50.86	0.40
45970.795	−55.81	0.39	**K827**			46296.902	−49.10	0.49
46053.801	−55.67	0.56	45995.852	−51.94	0.30	50277.840	−57.87	0.40
46419.874	−55.75	0.58	46296.916	−56.93	0.33			
			47445.793	−52.33	0.46	**K875**		
K758			48157.940	−59.03	0.65	45612.863	−55.13	...
46037.879	−20.22	0.46	48544.965	−61.01	0.51	46039.852	−56.59	0.78
			50037.651	−61.19	0.78	46419.900	−55.78	0.71
K765			50277.900	−57.53	0.40			
45712.619	−54.66	...				**K897**		
45970.790	−55.35	0.44	**K849**			45612.879	−53.04	...
46037.914	−57.27	0.40	45995.880	−52.92	0.54	46039.770	−52.42	0.78
46053.598	−57.24	0.49	46419.929	−50.85	4.52[a]	46053.773	−51.32	0.48

Table A.1: *Continued*

Name			Name			Name		
JD	Vel.	Err.	JD	Vel.	Err.	JD	Vel.	Err.
46296.956	−49.46	0.52	48950.914	−54.00	0.65	50361.942	−54.49	0.49
47081.981	−50.61	0.53	49269.976	−54.44	0.42			
48158.014	−50.55	0.50	50316.886	−55.23	0.59	**K1010**		
48545.007	−50.79	0.54				50276.871	−54.74	0.46
50344.780	−53.33	0.47	**K971**					
			45612.914	−53.74	···	**K1064**		
K902			46037.887	−54.60	0.40	50386.812	−12.27	2.28[a]
45990.876	−55.08	0.54	46100.785	−55.54	0.52			
46039.672	−53.75	0.67	46294.984	−55.20	0.39	**K1066**		
			46392.905	−54.17	0.78	45993.061	−54.57	0.53
K908			48950.933	−53.67	0.73	46039.684	−56.44	0.39
45612.898	−52.44	···	50030.887	−53.20	0.82	46295.991	−54.10	0.45
46039.805	−13.52	0.95[b]	50107.728	−55.10	0.65	47082.034	−55.31	0.70
46053.684	−51.19	0.35	50274.964	−54.82	0.24	47082.041	−55.84	0.62
46419.911	−56.28	0.66				48509.008	−54.16	0.40
48158.006	−61.58	0.56	**K977**			49269.983	−54.94	0.56
48545.029	−51.57	0.57	46039.824	−52.89	0.60	50344.686	−54.98	0.31
			47082.057	−52.32	0.53			
K950			47445.872	−53.59	0.39	**K1071**		
46052.800	−54.69	0.48	48509.020	−52.34	0.34	45962.932	−56.71	0.45
46380.822	−55.40	1.03[a]	48545.044	−52.22	0.32	46039.844	−56.78	0.58
48545.038	−56.24	0.64	48950.925	−52.17	0.83	46052.844	−55.41	0.52
			50030.869	−50.83	0.85	46380.803	−55.56	0.38
K957			50301.787	−50.17	0.24	50361.913	−56.21	0.50
46052.825	−54.81	0.46						
47445.010	−56.86	0.70	**K978**			**K1082**		
47445.016	−56.02	0.86	50387.715	−54.08	0.41	50278.934	−56.71	0.44
K970			**K991**			**K1091**		
45962.997	−54.78	0.37	46039.660	−11.99	0.47	45962.968	−54.22	0.44
46039.664	−56.09	0.67	50365.897	−12.15	0.66	46039.746	−54.93	0.58
46052.904	−55.52	0.47				46296.965	−53.99	0.61
46295.995	−54.21	0.44	**K1005**					
47082.022	−55.17	0.42	46039.734	−56.32	0.67	**K1092**		
48509.002	−54.54	0.60	47445.886	−53.89	0.49	46039.758	−66.42	0.64

Table A.1: *Continued*

Name			Name			Name		
JD	Vel.	Err.	JD	Vel.	Err.	JD	Vel.	Err.
47445.897	−65.71	0.57	46039.730	−56.06	0.52	**M580**		
			46392.873	−54.28	0.73	50386.677	−55.07	0.48
K1101			47082.050	−54.72	0.48			
45962.985	−54.61	0.41				**M748**		
46039.691	−54.91	0.38	**K1205**			50313.792	−66.50	0.36
46296.975	−54.21	0.46	50365.964	−23.32	0.58	50410.910	−66.22	2.05[a]
48509.013	−53.96	0.47						
			K1218			**M848**		
K1107			50366.004	−6.72	0.68	50313.908	−35.39	0.35
45962.950	−55.70	0.48						
46039.836	−56.60	0.52	**K1225**			**M866**		
46296.986	−57.38	0.56	46039.711	−42.65	0.59	50386.957	−54.27	1.84[a]
47445.909	−56.62	0.40				50422.687	−28.38	0.74
48545.060	−56.59	0.73	**K1244**					
			46039.723	−40.41	0.93	**M994**		
K1114						50365.870	−9.95	0.51
45612.926	−52.27	···	**K1312**					
47445.941	−53.77	0.55	50387.760	−55.18	0.43	**M959**		
						50361.835	−37.90	0.63
K1147			**M108**			50365.939	−39.04	0.48
50276.853	−55.47	0.35	50317.012	−2.05	0.51			
50365.666	−54.33	0.47				**M1121**		
			M125			50313.000	−55.63	0.63
K1149			50316.986	−24.23	0.67	50313.765	−55.60	0.49
46037.895	−43.16	0.75				50387.978	−55.61	0.49
47445.929	−45.98	0.49	**M193**			50410.836	−55.24	0.65
48545.051	−37.63	0.47	50313.745	−56.34	0.37			
50278.791	−37.60	0.41	50410.983	−57.64	1.71[a]	**M1244**		
						50387.646	−55.18	0.46
K1150			**M227**					
50386.641	−54.84	0.66	50313.846	−52.91	0.48			
K1196			**M215**					
45976.016	−54.54	0.33	50313.874	−57.37	0.51			
45993.045	−55.30	0.40						

VITA

Surname: GIM Given Names: MUNHWAN
Place of Birth: CheongJu, Korea(ROK)

Educational Institutions Attended:

University of Victoria	1993 to 1998
Yonsei University	1984 to 1990

Degrees Awarded

M.Sc.	Yonsei University	1990
B.Sc.	Yonsei University	1988

Honours and Awards

Yonsei University Fellowship	1984 to 1988
DongWeon Company Scholarship	1988 to 1990
Graduate Teaching Fellowship	1993 to 1994
Dean of Graduate Studies Scholarship	1994
University of Victoria Fellowship	1994 to 1995
Graduate Teaching Fellowship	1995 to 1998

PARTIAL COPYRIGHT LICENSE

I hereby grant the right to lend my thesis to users of the University of Victoria Library, and to make single copies only for such users or in response to a request from the Library of any other university, or similar institution, on its behalf or for one of its users. I further agree that permission for extensive copying of this thesis for scholarly purposes may be granted by me or a member of the University designated by me. It is understood that copying or publication of this thesis for financial gain shall not be allowed without my written permission.

Title of Thesis:

A Photometric and Radial-Velocity Study of the Open Cluster NGC 7789

Author: [redacted]

Munhwan Gim

July 19, 1998